Click Here for Full Article

Calculating bed load transport in steep boulder bed channels

E. M. Yager,[1,2] J. W. Kirchner,[1] and W. E. Dietrich[1]

Received 17 August 2006; revised 27 February 2007; accepted 30 March 2007; published 13 July 2007.

[1] Steep, rough channels occupy a large fraction of the total channel length in mountainous regions. Most sediment mobilized on hillslopes must pass through these streams before reaching lower-gradient channels. Steep channels have wide grain size distributions that are composed of finer, more mobile sediment and large, rarely mobile grains. The large grains can bear a significant portion of the total shear stress and thereby reduce the stress available to move the finer sediment. Conventional bed load transport equations often overpredict the sediment flux in steep channels by several orders of magnitude. We hypothesize that sediment transport equations overpredict the sediment flux because they do not (1) account for the stress borne by rarely mobile grains, (2) differentiate between highly and rarely mobile sediment, and (3) account for the limited availability of mobile sediment. Here we modify a conventional bed load transport equation to include these three effects. We use measurements of the flow, bed properties, and sediment flux in a small, steep flume to test this equation. We supply gravel at a constant rate through fields of regularly spaced immobile spheres and measure the bed coverage by gravel and sphere protrusion (the percent of the sphere that protrudes above the gravel deposit). For a given sphere spacing, the proportion of the bed covered by gravel increases and the sphere protrusion decreases with greater sediment supply. Thus bed coverage and immobile grain protrusion may serve as proxies for sediment availability in steep, rough streams. Unlike most transport equations that we tested, our modified bed load equation predicts sediment fluxes to within an order of magnitude of the measured values. Our results demonstrate that accurately predicting bed load transport in steep, rough streams may require accounting for the effects of local sediment availability (coverage by mobile sediment) and drag due to rarely mobile particles.

Citation: Yager, E. M., J. W. Kirchner, and W. E. Dietrich (2007), Calculating bed load transport in steep boulder bed channels, *Water Resour. Res.*, *43*, W07418, doi:10.1029/2006WR005432.

1. Introduction

[2] The majority of the total channel length in mountainous watersheds occurs in steep (gradients greater than 3 percent), rough channels. Steep channels differ from downstream, lower-gradient reaches in several distinct ways. They have smaller drainage areas and steeper bed slopes, which together cause the ratio of the flow depth to the grain size to be small. The wide grain-size distribution includes patches of finer, more mobile sediment and large, relatively immobile boulders that are often arranged into cascades or steps (Figure 1). Annual snowmelt and stormflows can mobilize fine sediment while boulders only move in rare, larger floods or debris flows. In reaches with gradients steeper than 10%, sediment transport and valley incision may occur primarily by occasional debris flows [*Stock and Dietrich*, 2003, 2006]. In steep channels, the large, relatively immobile grains disrupt the flow [e.g., *Bathurst*, 1978; *Wiberg and Smith*, 1991; *Byrd and Furbish*, 2000; *Byrd et al.*, 2000; *Wohl and Thompson*, 2000], increase turbulence [*Papanicolaou et al.*, 2001] and alter channel roughness [e.g., *Bathurst*, 1985; *Wiberg and Smith*, 1991; *Marcus et al.*, 1992]. Such flow complexity causes conventional resistance equations to predict flow velocities that, on average for a given channel, differ from the measured values by anywhere from 20% to an order of magnitude [e.g., *Bathurst*, 1985; *Marcus et al.*, 1992; *Bathurst*, 2002; *Katul et al.*, 2002]. The velocity profile is commonly not logarithmic [*Wiberg and Smith*, 1991; *Byrd and Furbish*, 2000; *Byrd et al.*, 2000; *Wohl and Thompson*, 2000], which precludes using the law of the wall to predict the flow velocity (and therefore the bed shear stress). The large grains also cause local flow accelerations [e.g., *Thompson*, 2007; *Wilcox and Wohl*, 2007], large spatial variations in velocity and stress [e.g., *Thompson*, 2007; *Wilcox and Wohl*, 2007], hydraulic jumps, and aeration [e.g., *Vallé and Pasternack*, 2006] further complicating stress predictions.

[3] Many studies of flow in steep channels have focused on the effects of large grains and their incorporation into resistance equations. Field and flume data indicate that particle resistance is inversely related to the spacing between large grains [*Judd and Peterson*, 1969; *Bathurst*, 1978; *Bathurst et al.*, 1981; *Ferro*, 1999] and the degree of particle submergence in the flow [e.g., *Keulegan*, 1938; *Judd and Peterson*, 1969; *Bathurst*, 1978; *Thompson and*

[1]Department of Earth and Planetary Science, University of California, Berkeley, California, USA.
[2]Now at School of Geographical Sciences, Arizona State University, Tempe, Arizona, USA.

Copyright 2007 by the American Geophysical Union.
0043-1397/07/2006WR005432$09.00

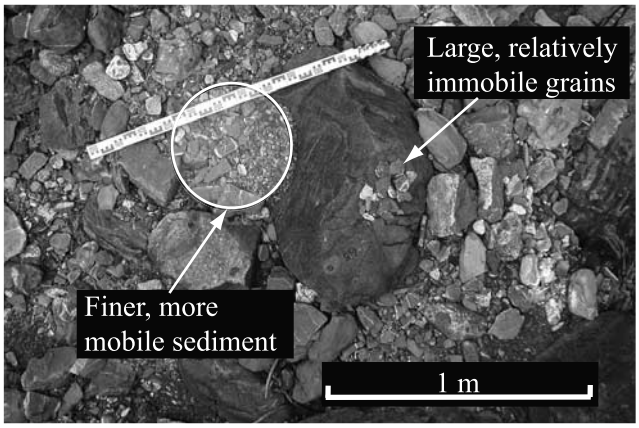

Figure 1. Bed of the Erlenbach Torrent in Switzerland. The bed of this small (0.74 km^2 drainage area), steep (10% gradient) stream is divided between finer, more mobile gravel and large, relatively immobile boulders.

Campbell, 1979; *Bathurst et al.*, 1981; *Jarrett*, 1984; *Ferro*, 1999; *Lee and Ferguson*, 2002]. Some have argued that resistance equations should include the additional effects of channel slope [*Jarrett*, 1984], Froude number [*Bathurst et al.*, 1981; *Bathurst*, 1985; *Rosso et al.*, 1990; *Ferro*, 1999], Reynolds number [*Bathurst et al.*, 1981], sediment mobility [*Bathurst*, 1985; *Ferro*, 1999], channel geometry [*Bathurst et al.*, 1981], and aeration [*Scheuerlein*, 1973; *Vallé and Pasternack*, 2006].

[4] A number of studies have included the effects of large grains in resistance equations [e.g., *Judd and Peterson*, 1969; *Bathurst*, 1978; *Thompson and Campbell*, 1979; *Bathurst et al.*, 1981; *Jarrett*, 1984; *Bathurst*, 1985; *Aguirre-Pe and Fuentes*, 1990; *Rosso et al.*, 1990; *Rickenmann*, 1994; *Ferro*, 1999; *Lee and Ferguson*, 2002]. These empirical expressions need to be recalibrated to each stream in which they are used, thus restricting their wider applicability. Somewhat more general results have been achieved from theoretical models that use stress partitioning [*Wiberg and Smith*, 1991; *Lawrence*, 1997, 2000] or mixing layer theory [*Katul et al.*, 2002] to account for the resistance due to large grains. Velocity profiles predicted from one such model [*Wiberg and Smith*, 1991] agreed with the measured profiles in channels with gradients less than three percent.

[5] In addition to complex hydraulics, steep streams also have a wide range of grain sizes that move through a variety of mechanisms and over a range of timescales. Steep streams receive an irregular supply of sediment from episodic landslides, bank failures and debris flows [*Bathurst*, 1985]. Finer material is selectively transported in steep channels [*Lenzi et al.*, 1999; *Laronne et al.*, 2001; *Lenzi*, 2001] with dimensionless critical shear stresses as high as 0.1 [e.g., *Bathurst et al.*, 1987; *Lenzi et al.*, 2006] (as compared to 0.035 to 0.06 [*Buffington and Montgomery*, 1997] in lower-gradient channels). In steep streams the critical shear stress may depend on the channel slope and the relative submergence (ratio of flow depth to grain size) [*Ashida and Bayazit*, 1973; *Aguirre-Pe*, 1975; *Mizuyama*, 1977; *Bathurst et al.*, 1979; *Bathurst*, 1987; *Bathurst et al.*, 1987; *Graf and Suszka*, 1987; *Wiberg and Smith*, 1987; *Buffington and Montgomery*, 1997; *Lenzi*, 1999; *Lenzi et al.*, 2006]. The apparently large critical shear stresses may be caused by the immobile grains because they (1) exert drag on the flow, reducing the stress available to transport the finer sediment [e.g., *Buffington and Montgomery*, 1997] and (2) locally shelter the bed from high shear stresses [e.g., *Wiberg and Smith*, 1991]. Thus, even the finer sediment, which should be relatively mobile, can be difficult to move in steep, rough channels. Conventional sediment transport equations, developed for lower-gradient reaches, typically overpredict sediment flux in steep streams by several orders of magnitude [e.g., *Bathurst et al.*, 1987; *Rickenmann*, 1997; *D'Agostino and Lenzi*, 1999]. Sediment transport equations derived for steep channels [e.g., *Smart*, 1984; *Bathurst et al.*, 1987; *Graf and Suszka*, 1987; *Aziz and Scott*, 1989; *Rickenmann*, 1997; *Lenzi et al.*, 1999] also overpredict sediment flux. Most bed load transport equations perform better in large flow events where the excess shear stress is very high and all sediment sizes become mobile [*Bathurst et al.*, 1987; *Rickenmann*, 1997; *D'Agostino and Lenzi*, 1999]. The poor performance of sediment transport equations limits our ability to model bedrock incision, to calculate sediment routing through a watershed, and to determine the downstream effects of land use practices on hillslopes.

[6] Here, we develop and experimentally test a set of coupled flow and sediment transport equations to predict the rate of gravel transport through steep, boulder bed streams. We modify a conventional sediment transport equation to incorporate the effects of immobile grains and reduced sediment availability. We can use this equation to predict sediment transport rates from measurements of the spacing, diameter, and protrusion of immobile grains, combined with the channel slope, channel width, water discharge, and mobile grain size.

2. Theory Development

[7] Large, relatively immobile grains cause local accelerations and decelerations in the flow, hydraulic jumps, large vertical velocities, localized intense turbulence, and areas of eddying water with weak net flow. A model with spatially and temporally varying stresses and sediment fluxes could theoretically describe the complexity of steep streams. This is currently a daunting computational task and would not be generally applicable for use in the field and in calculations of sediment routing through watersheds. We therefore focus on the reach-averaged flow and bed properties to predict sediment transport in steep streams.

[8] We simplify the bed into regularly arranged immobile grains with intervening finer, more mobile sediment. We hypothesize that the drag borne by the exposed immobile grains will significantly reduce the stress on the mobile sediment. Furthermore, the protrusion of, and therefore the stress borne by, the immobile grains should increase as the sediment supply declines. We assume that the portion of the bed covered by mobile sediment should vary directly with sediment supply. For example, as the sediment supply declines below the transport capacity, mobile grains will be progressively eroded from the bed.

[9] We develop an equation to partition the total stress [e.g., *Schlichting*, 1936; *Einstein and Banks*, 1950; *Raupach*, 1992; *Raupach et al.*, 1993; *Shields and Gippel*, 1995; *Manga and Kirchner*, 2000; *Stone and Shen*, 2002] between that borne by the immobile and mobile fractions. Although

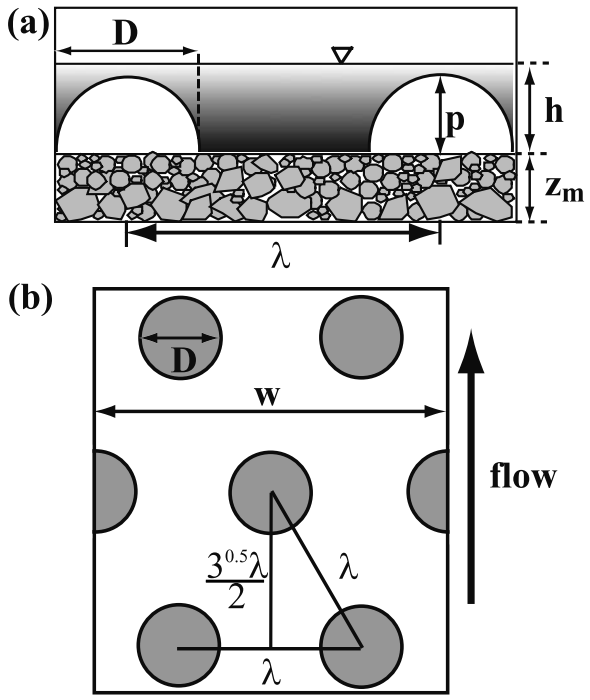

Figure 2. Bed geometry used in flume experiments and in stress-partitioning calculations. Idealized channel in (a) cross-section and (b) plan view. Here p is the portion of the immobile grain diameter that is above the mobile sediment deposit, D is the immobile grain diameter, z_m is the height of the mobile sediment deposit, h is the flow depth between immobile grains, w is the channel width, and λ is the spacing between immobile grains.

this stress-partitioning approach may overestimate the stress borne by individual fractions [see *Wilcox et al.*, 2006], it still provides a relatively good estimate of the stress on the mobile sediment. Our stress-partitioning equation was derived for reaches without significant quantities of woody debris or step-pool structures, which can also bear a large portion of the total shear stress [e.g., *Curran and Wohl*, 2003; *Wilcox et al.*, 2006]. We make three modifications to bed load transport equations that use the excess shear stress: (1) We use the median grain size of the mobile fraction as the representative bed load size, (2) we only use the portion of the shear stress that acts on the mobile sediment, and (3) we scale the predicted flux by the portion of the bed covered by mobile grains.

[10] We developed our theory independently from a similar approach [*Jordanova and James*, 2003] that also uses the stress on the mobile sediment to predict bed load fluxes. Unlike the theory of Jordanova and James, our theory accounts for the variable submergence of the immobile grains and the availability (and thickness) of the mobile sediment. Furthermore, the theory of Jordanova and James was empirically calibrated to flume experiments and was not developed for steep channels. Our stress-partitioning equation may be considered a modified version of the equations developed by *Wiberg and Smith* [1991] for sediment transport predictions. However, to predict the flow hydraulics, we only require the water discharge (to predict the depth-averaged velocity) whereas the *Wiberg and Smith* [1991] approach requires the flow depth and water discharge (to obtain a velocity profile). Our goal is to use bed grain size distributions, the spacing and size of immobile grains, the channel slope, and an expected discharge to predict the transport rate of the finer, mobile sediment.

2.1. Stress Partitioning

[11] We divide the bed into two fractions, immobile grains with a characteristic spacing (λ) and diameter (D), and mobile sediment represented by a median grain size (D_{50m}) (Figure 2). Given these assumptions, we partition the total boundary shear stress (τ_t) between the stress on the large, immobile grains (τ_I) and the stress on the finer, more mobile bed (τ_m):

$$\tau_t A_t = \tau_I A_{IP} + \tau_m A_m \tag{1a}$$

$$\tau_t = \frac{\tau_I A_{IP} + \tau_m A_m}{A_t}, \tag{1b}$$

where A_t is the total bed area (see section 2.2 for area calculations) occupied by both the mobile and immobile grains, A_{IP} is the bed-parallel area of the immobile grains (within A_t), and A_m is the bed-parallel area of the mobile sediment (within A_t). Equation (1a) states that the total fluid shear force on the bed is equal to the sum of the drag on the mobile and immobile grains. We assume that the wall roughness in steep channels is relatively unimportant compared to the resistance caused by the mobile and immobile grains. Steep streams may also have moderate width-to-depth ratios (Table 1) during sediment transporting flows. Thus we neglect the resistance due to walls in equation (1). We assume reach-averaged steady, uniform flow and calculate the total boundary shear stress as the bed-parallel component of the downstream pressure gradient,

$$\tau_t = \rho g h_a S, \tag{2}$$

in which ρ is the density of water, g is the acceleration due to gravity, h_a is the average flow depth and S is the reach-averaged water surface slope. We neglect the local variations in the flow depth and velocity by approximating steady, uniform flow over a long study reach (about 10–20 channel widths). We calculate τ_m as the drag force of the mobile grains divided by their bed-parallel area:

$$\tau_m = \frac{\rho C_m U^2}{2}, \tag{3}$$

where U is the reach-averaged velocity and C_m is the drag coefficient for the mobile sediment. The bed-parallel area cancels out of equation (3). Similarly, τ_I is the drag force of the immobile grains divided by their total bed-parallel area:

$$\tau_I = \frac{\rho A_{IF} C_I U^2}{2 A_{IP}}, \tag{4}$$

where C_I is the drag coefficient for the immobile grains and A_{IF} is the bed-perpendicular area of immobile grains (within A_t). The velocities experienced by the immobile and mobile grains should be very different because the large grains

Table 1. Measured Flow Conditions in Steep, Rough Channels[a]

Slope, %	D_{84}, mm	Q, m^3/s	U, m/s	h_a, m	h_a/D_{84}	w/h_a	Fr	Stream	Source
7–19.7	56–121	0.52–0.98	0.55–1.07	0.19–0.35	1.6–4.7	6–23	0.34–0.73	E. St. Louis Cr.	*Adenlof and Wohl* [1994]
11–14	N/A–660	4	1.93–1.95	0.42–0.48	N/A–0.6	N/A	0.89–0.96	Rio Cordon	*Lenzi* [2001]
11.2–14.6	84–114	0.01–0.47	0.2–0.91	0.05–0.24	0.4–2.6	9–15	0.29–0.65	Unnamed (1–3)	*Lepp et al.* [1993]

[a]Measured slope (%), grain size (D_{84}), discharge (Q), velocity (U), channel width (w), reach-averaged flow depth (h_a), relative submergence (h_a/D_{84}), and Froude number (Fr) for five steep channels during sediment transport events. For Lenzi data, we report the D_{50} of steps of large grains because the reach-averaged D_{84} was not reported. We exclude any data from Lepp et al. and Lenzi that were not measured during sediment transport events.

protrude significantly into the flow. However, we use the same reach-averaged velocity in both (3) and (4) to make the system of equations solvable; introducing another velocity would add too many unknowns. Instead, we assume that the relatively low velocity felt by the mobile grains can be incorporated into the drag coefficient of the mobile sediment (see section 4.1 for measurement of C_m). We now derive how each area term varies with the flow depth and the thickness of the mobile sediment.

2.2. Area Calculations

[12] We assume spherical immobile grains to simplify the calculation of immobile grain areas. We arrange the bed into a staggered pattern of immobile grains with a regular diagonal and cross-stream spacing (λ) as shown in Figure 2. From this specific geometry we derive equations for A_t, A_m and V_w (see section 2.3). The downstream spacing between immobile grains is our only geometry-specific parameter and may need to be changed for other bed geometries. Here we define the total bed area as

$$A_t = \frac{\sqrt{3}\lambda}{2} w. \tag{5}$$

The total bed area is the product of the width and the downstream spacing, where the downstream spacing is slightly less than λ because of the staggered pattern of immobile grains (Figure 2). The total bed area is not equivalent to the total reach area; it the total representative area of the bed that repeats in the downstream direction. Although our calculations are independent of the reach length, they use reach-averaged properties.

[13] The number of immobile grains within A_t is equal to w/λ where w is the channel width. The bed-perpendicular area of the immobile grains (A_{IF}) is given by

$$\mathrm{A_{IF}} = \left[\left(\mathrm{h}+\mathrm{z_m}-\frac{\mathrm{D}}{2}\right)\sqrt{(\mathrm{h}+\mathrm{z_m})\mathrm{D}-(\mathrm{h}+\mathrm{z_m})^2} + \frac{\mathrm{D}^2}{4}\sin^{-1}\left(2\left(\frac{\mathrm{h}+\mathrm{z_m}}{\mathrm{D}}\right)-1\right) - \left(\mathrm{z_m}-\frac{\mathrm{D}}{2}\right)\sqrt{\mathrm{z_m D}-\mathrm{z_m^2}}\ \right]\frac{\mathrm{w}}{\lambda} - \frac{\mathrm{D}^2\mathrm{w}}{4\lambda}\sin^{-1}\left(\frac{2\mathrm{z_m}}{\mathrm{D}}-1\right) \quad \text{when } h+z_m \le D \tag{6a}$$

$$\mathrm{A_{IF}} = \left[\frac{\pi\mathrm{D}^2}{8} - \left(\mathrm{z_m}-\frac{\mathrm{D}}{2}\right)\sqrt{\mathrm{z_m D}-\mathrm{z_m^2}} - \frac{\mathrm{D}^2}{4} \cdot \sin^{-1}\left(\frac{2\mathrm{z_m}}{\mathrm{D}}-1\right)\right]\frac{\mathrm{w}}{\lambda} \quad \text{when } h+z_m \ge D. \tag{6b}$$

where z_m is the bed-perpendicular height of the mobile sediment above the base of the immobile grains, and h is the flow depth between immobile grains (see Figure 2). Equation (6a) is derived by integrating the equation for a circle between lines for the height of the mobile sediment and the flow depth (h). The flow depth (h) is measured from the top of the mobile sediment deposit to the water surface. When the flow overtops the immobile grains, we integrate the equation for a circle from the height of the mobile sediment to the top of the grain to yield (6b). The bed-parallel area of the immobile grains (A_{IP}) is

$$A_{IP} = \frac{\pi D^2 w}{4\lambda} \quad \text{when } z_m/D \le 0.5 \tag{7a}$$

$$A_{IP} = \frac{\pi z_m (D-z_m) w}{\lambda} \quad \text{when } z_m/D \ge 0.5. \tag{7b}$$

A_{IP} remains constant when z_m is below the immobile grain centerline (7a), and varies with z_m when z_m is above the immobile grain centerline (7b). The total area occupied by the mobile fraction (A_m) is the difference between the total bed area and the area occupied by immobile grains:

$$A_m = \frac{w\sqrt{3}\lambda}{2} - A_{IP}. \tag{8}$$

2.3. Average Flow Depth

[14] The average flow depth (h_a) is often calculated as the cross-sectional area of the flow divided by the channel width. Here we calculate the average flow depth as the total water volume (within one downstream spacing between the immobile grains) divided by the total bed area. The total water volume (V_w) is the difference between the total volume (water and immobile grains) and the volume of immobile grains:

$$V_w = \frac{w\sqrt{3}\lambda h}{2} - V_I. \tag{9}$$

The total volume is the product of the width, flow depth between immobile grains, and downstream immobile grain spacing. The total volume of the immobile grains (V_I) is given by

$$\mathrm{V_I} = \frac{\mathrm{w}\pi\mathrm{h}}{\lambda}\left(\mathrm{z_m}(\mathrm{D}-\mathrm{z_m}-\mathrm{h})+\mathrm{h}\left(\frac{\mathrm{D}}{2}-\frac{\mathrm{h}}{3}\right)\right) \text{when } h+z_m < D \tag{10a}$$

$$\mathrm{V_I} = \frac{\mathrm{w}\pi}{\lambda 6}\left(\mathrm{D}^3 - 3\mathrm{z_m^2 D} + 2\mathrm{z_m^3}\right) \quad \text{when } h+z_m > D. \tag{10b}$$

The reach-averaged flow depth (h_a) is then given by

$$h_a = \frac{V_w}{A_t}. \quad (11)$$

2.4. Solution of Stress-Partitioning Equations

[15] We use the continuity equation to write that the reach-averaged velocity (U) is the discharge divided by the average cross-sectional area of the flow,

$$U = \frac{qw}{\left(\frac{2V_w}{\sqrt{3}\lambda}\right)}, \quad (12)$$

where q is discharge per unit width. The average cross-sectional area is the total water volume divided by the downstream spacing between immobile grains. Combining (1)–(5), (11) and (12) gives an equation for discharge:

$$q = \sqrt{\frac{8gSV_w^3}{3\lambda^2 w^2(A_{IF}C_I + A_m C_m)}}. \quad (13)$$

To solve (13), we assume a discharge and must iterate to determine the flow depth between the immobile grains (h) because it enters the equation through A_{IF} (equation (6)) and V_w (equation (9)). The flow velocity and the stress on the mobile sediment are calculated with this flow depth and equations (12) and (3), respectively. The stress on the mobile sediment is then used to predict the sediment transport rate. To solve (13) we need to specify six reach-averaged variables (w, S, q, D, z_m, and λ) and two coefficients (C_m and C_I).

2.5. Bed Load Transport Calculations

[16] We modify conventional, stress-based bed load equations (1) to use the stress on the mobile sediment rather than the total boundary shear stress, (2) to use the median mobile grain size rather than the median grain size of the entire bed, and (3) to scale the transport rate by the proportion of the bed occupied by the mobile sediment. We use the *Fernandez Luque and Van Beek* [1976] equation as an example here:

$$q_s^* = 5.7(\tau_t^* - \tau_c^*)^{1.5}, \quad (14)$$

in which

$$q_s^* = \frac{q_s}{\left[\left(\frac{\rho_s}{\rho} - 1\right)gD_{50}^3\right]^{0.5}} \quad (15)$$

$$\tau_t^* = \frac{\tau_t}{(\rho_s - \rho)gD_{50}} \quad (16)$$

$$\tau_c^* = \frac{\tau_c}{(\rho_s - \rho)gD_{50}}. \quad (17)$$

The dimensionless sediment transport rate (q_s^*) is a function of the excess shear stress ($\tau_t^* - \tau_c^*$), where τ_c^* is the dimensionless critical shear stress and τ_t^* is the dimensionless total shear stress. Here q_s is the volumetric transport rate per unit width, ρ_s is the density of sediment, and D_{50} is the median grain size. The critical shear stress (τ_c) is the stress needed to mobilize the median grain size on the channel bed.

[17] We replace τ_t with τ_m and use the median grain size of the mobile fraction (D_{50m}), hence

$$q_{sm}^* = 5.7(\tau_m^* - \tau_{cm}^*)^{1.5}, \quad (18)$$

where

$$q_{sm}^* = \frac{q_{sm}}{\left[\left(\frac{\rho_s}{\rho} - 1\right)gD_{50m}^3\right]^{0.5}} \quad (19)$$

$$\tau_m^* = \frac{\tau_m}{(\rho_s - \rho)gD_{50m}} \quad (20)$$

$$\tau_{cm}^* = \frac{\tau_{cm}}{(\rho_s - \rho)gD_{50m}}. \quad (21)$$

In equations (18)–(21), q_{sm}^* is the dimensionless transport rate of the mobile sediment, q_{sm} is the volumetric transport rate of the mobile sediment per unit width, τ_{cm}^* and τ_{cm} are the dimensionless critical and critical shear stresses of the mobile sediment, and τ_m^* is the dimensionless stress borne by the mobile sediment. To account for the limited availability of mobile sediment, we scale the predicted transport rate by the proportion of the bed area that is occupied by the mobile fraction. Thus (18) becomes

$$q_{sm}^* = 5.7(\tau_m^* - \tau_{cm}^*)^{1.5}\frac{A_m}{A_t}. \quad (22)$$

[18] Although we use the Fernandez Luque and Van Beek equation because of its relative simplicity, we could also modify most bed load transport equations in a similar fashion (see Appendix C). We now test the sensitivity of our flow and sediment flux predictions to the various parameters in our stress-partitioning and sediment transport equations.

3. Predicted Effects of Large, Immobile Grains on Hydraulics and Sediment Transport

[19] For a given channel, the spacing (λ), size (D), and protrusion (P) of the immobile grains partially determine the stress available to move the mobile sediment. Protrusion is the distance from the top of the immobile grain to the average bed surface between immobile grains (Figure 2), and is expressed as a fraction of the total grain diameter (($D - z_m$)/D); multiplying by 100 gives protrusion as a percentage of the diameter. The immobile grain diameter and spacing are relatively static on an annual basis, while the protrusion should vary from year to year with the supply of mobile sediment.

[20] We plot the flow hydraulics (U, h_a, h) and sediment transport rates as functions of two dimensionless parame-

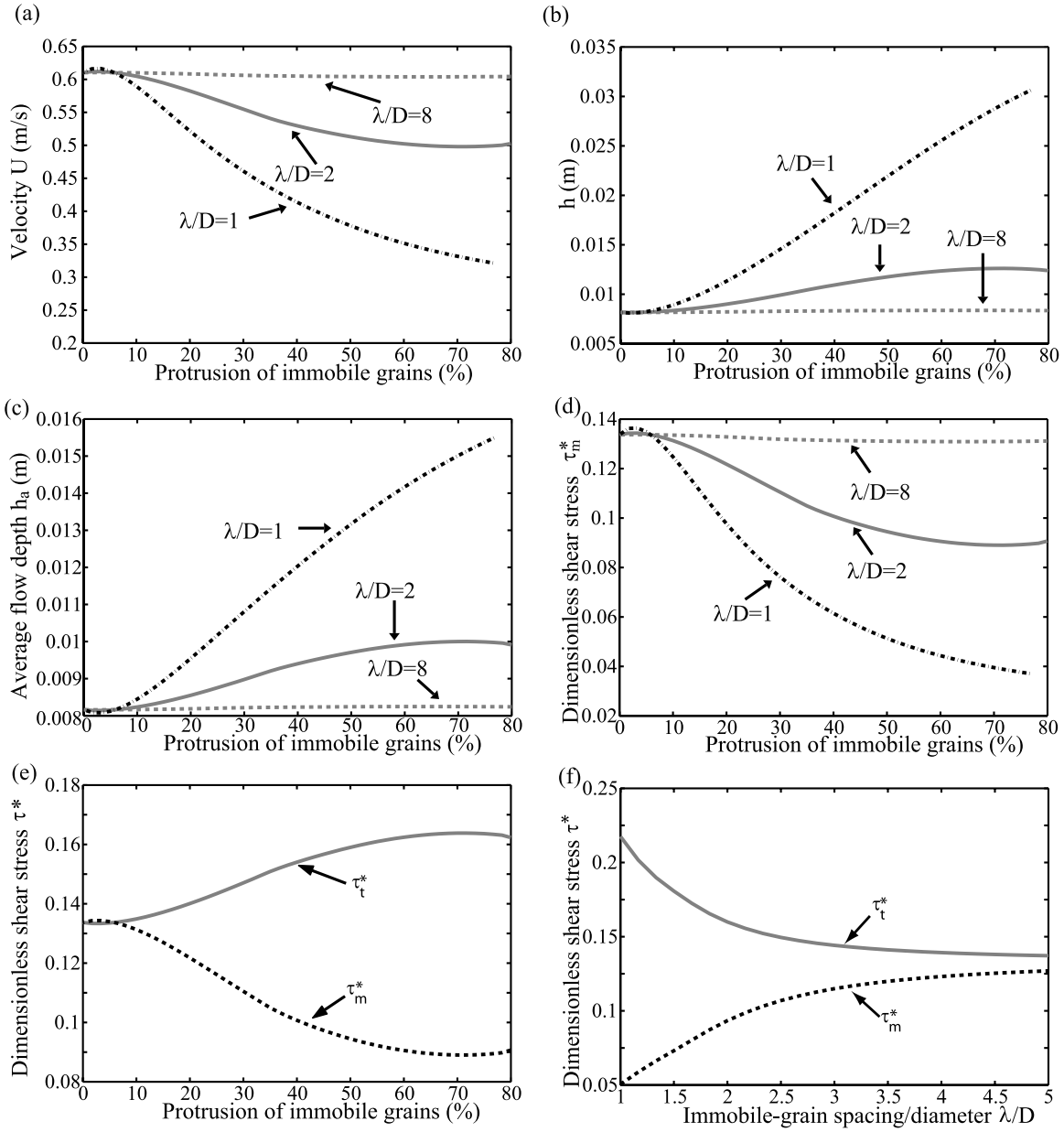

Figure 3. Stress-partitioning predictions as a function of the immobile grain protrusion: (a) flow velocity, (b) flow depth between immobile grains, (c) average flow depth, (d) dimensionless stress on the mobile sediment, and (e) dimensionless total stress and stress on the mobile sediment for λ/D of 2. (f) Variation of the dimensionless stresses (for 50% protrusion) with λ/D. All other parameters are held constant (q = 0.0049 m^2/s, S = 0.10, C_m = 0.047, and C_I = 0.4).

ters, λ/D (dimensionless spacing) and P. We vary λD and P independently (while holding D constant) although P may change with λ. In our plots, λ/D ranges from 1 (closely packed bed) to 8 (widely spaced immobile grains), and P ranges from zero to 80% because most immobile grains are partially buried. We assume constant values of 0.047 for C_m (see section 4.1) and 0.4 for C_I (sphere in a free stream [*Munson et al.* [1998]) and hold all other parameters constant at the values used in our flume experiments (see section 4.1).

3.1. Hydraulic Variables' Dependence on λ and P

[21] For a given λ/D, an increase in protrusion roughens the bed and therefore decreases the flow velocity (Figure 3a), and increases the average flow depth (Figure 3c) and the depth between the immobile grains (Figure 3b). For a given P, an increase in λ/D (fewer immobile grains) causes the velocity to increase (Figure 3a) and the average flow depth to decrease (Figure 3c). An increase in P or decrease in λ/D causes more stress to be borne by the immobile grains and the stress on the mobile sediment (equation (3)) to decline (Figure 3d). When protrusion is relatively large or immobile grains are relatively frequent ($\lambda/D < 3$), the stress on the mobile sediment is significantly reduced (Figures 3e and 3f). The range of λ/D (1 to 3) that is most effective at reducing the stress on the mobile sediment is what we commonly observe in steep channels. More widely spaced and/or more

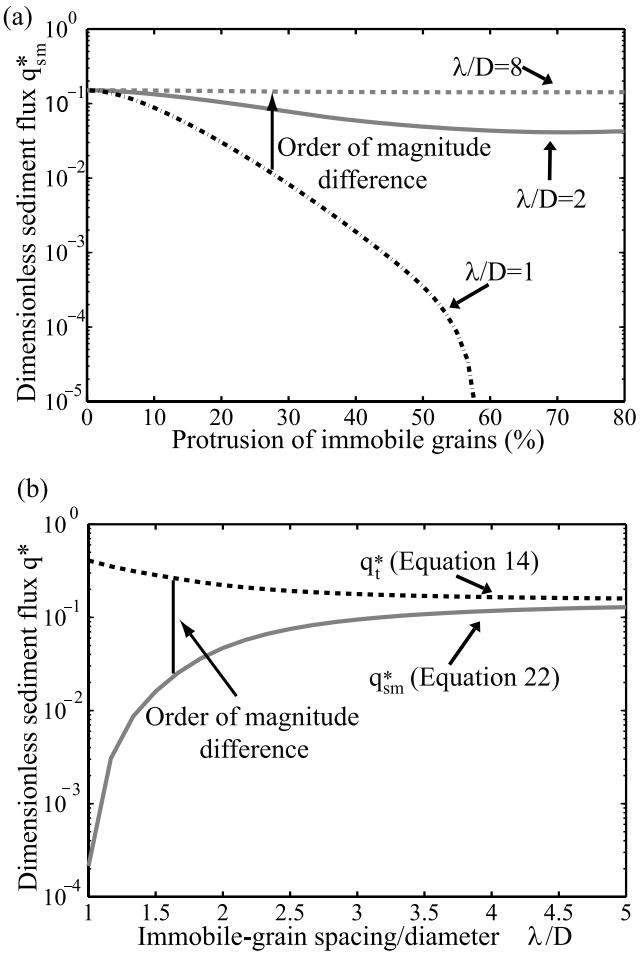

Figure 4. (a) Calculated dimensionless transport rates (equation (22)) as a function of immobile grain protrusion for a range of λ/D. (b) Dimensionless sediment fluxes as a function of λ/D (for 50% protrusion). All parameters are held constant (q = 0.0049 m^2/s, S = 0.10, C_m = 0.047, C_I = 0.4, D_{50m} = 0.0037 m, and τ^*_c = 0.045) at values representative of our flume experiments.

buried immobile grains do not effectively reduce the average stress borne by the mobile sediment.

[22] In our calculations, beds with very low λ/D cause the greatest flow resistance (for a given P) because we assume a constant value of C_I in equation (4). Previous flume experiments and theoretical calculations have demonstrated that a small decrease in spacing (from widely spaced grains) will augment the bed roughness and cause the flow to slow and deepen. Any further decrease in spacing will cause the immobile grain wakes to significantly overlap (skimming flow) and the bed to become relatively smooth. Thus an intermediate spacing between immobile grains may cause the greatest flow resistance [e.g., *Einstein and Banks*, 1950; *Morris*, 1955; *Rouse*, 1965; *Li and Shen*, 1973; *Raupach* 1992; *Raupach et al.*, 1993; *Nepf*, 1999; *Lawrence*, 2000; *King et al.*, 2005]. We do not include these effects in our calculations because, to best of our knowledge, the variation of C_I with immobile grain spacing is not yet predicted by any general theory.

3.2. Bed Load Transport Calculations

[23] We calculate sediment transport rates using equations (14) and (22), which are the original and our modified versions of the Fernandez Luque and Van Beek equation, respectively. Equation (22) accounts for the limited availability of the mobile sediment and only uses the stress on the mobile sediment (as calculated in section 3.1). Equation (14) uses the total shear stress calculated from stress partitioning. For the dimensionless critical shear stresses in each equation (τ^*_{cm} and τ^*_c), we assume the commonly used value for gravel bed rivers of 0.045 [*Buffington and Montgomery*, 1997].

[24] When immobile grains are widely spaced, they bear a small portion of the total stress and cover a relatively small area of the bed. Thus, when λ/D is greater than 2, both the availability of, and the stress borne by, the mobile sediment are high and the transport rates from (14) and (22) are similar (Figure 4b). Furthermore, protrusion has little effect on the predicted sediment transport rates when grains are very widely spaced (Figure 4a). The stress borne by, and coverage of, the mobile sediment significantly decrease with lower λ/D when the immobile grains are closely spaced ($\lambda/D < 2$). When λ/D is less than 2, the sediment transport rates predicted by (22) are at least an order of magnitude lower than those predicted by (14) (Figure 4b). The stress on the mobile sediment is close to the critical stress when λ/D is low; the excess shear stress declines with decreasing λ/D. The sediment transport rates predicted from (22) rapidly decrease because of this decline in excess shear stress (Figure 4b).

4. Flume Experiments

4.1. Experiment Design

[25] We designed a set of flume experiments with a simple, well-defined bed configuration to test our modified sediment transport equation. The experiments were con-

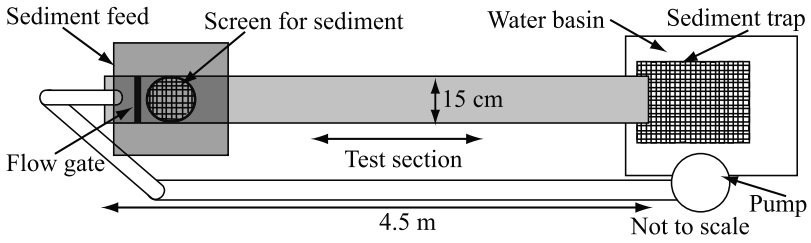

Figure 5. Schematic of the experimental apparatus. Water is pumped to the upstream end of the flume and is contained behind a flow gate. Sediment enters the flume just downstream of the gate and is captured in a trap at the downstream end of the flume. All measurements took place in the center test section of the flume.

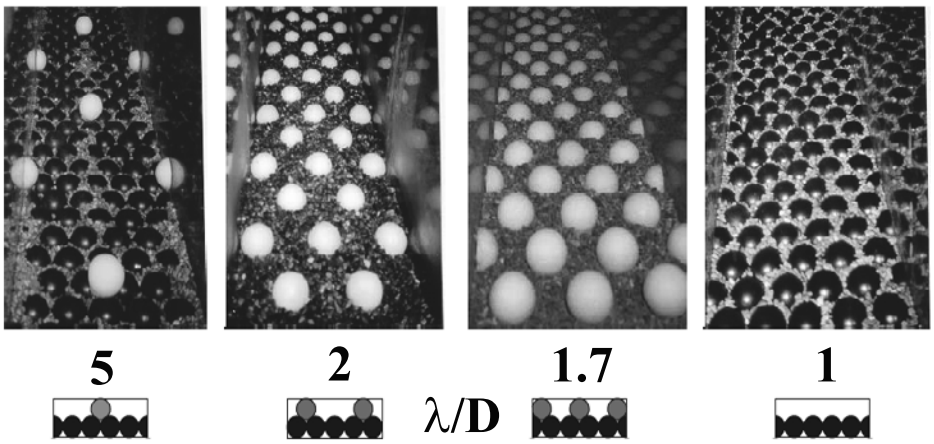

Figure 6. Photographs of the beds of spheres (0.03 m diameter) used in the flume experiments; λ/D varies on the top layer (white) and is constant on the bottom layer (black). Diagrams of each bed in cross section are below the photos.

ducted in a small (15 cm wide, 4.5 m long) flume set at a gradient of ten percent (Figure 5). This is the steepest gradient at which fluvial processes have been hypothesized to dominate over debris flow scour and deposition [*Stock and Dietrich*, 2003, 2006]. At this gradient, the influence of the immobile grains on the flow and sediment transport will be relatively large. Thus our experiments should provide a test of sediment transport equations at the limit of their applicability. We maintained a constant slope in our experiments to enable comparisons between all experimental runs. The flume bed consisted of two layers of 30 mm immobile spheres: a closely packed bottom layer (λ/D of 1) and a top layer in which λ/D varied from 1 to 5 in the different runs (Figure 6).

[26] The Reynolds number and particle Reynolds number (based on 30 mm spheres) were scaled to ensure fully developed turbulent and hydraulically rough flow. We also scaled our experiments using the few hydraulic data (Table 1) that exist for sediment transporting flows in steep (gradients >5%), rough streams [*Lepp et al.*, 1993; *Adenlof and Wohl*, 1994; *Lenzi*, 2001]. The relative submergence of the exposed immobile grains in our flume ($h_a/[D - z_m]$ of 0.3 to 2.2) was scaled to fall within the range of values (h_a/D_{84} of 0.4 to 5.6) measured by *Lepp et al.* [1993], *Adenlof and Wohl* [1994], and *Lenzi* [2001].

[27] In our experiments, we only approximately scaled the Froude number ($Fr = U/[gh_a]^{0.5}$) (Fr of 1 to 4) to the upper range of values (Fr of 0.3 to 1) observed by *Lepp et al.* [1993], *Adenlof and Wohl* [1994], and *Lenzi* [2001]. Although local flow transitions (hydraulic jumps) occurred downstream of each sphere, the reach-averaged Froude number was greater than one in all experiments because of the steep bed slope and shallow flow. The Froude number was between 1 and 1.6 for beds that most resembled steep streams in the spacing between the immobile grains (λ/D of 1.7 and 2). Reach-averaged Froude numbers that are greater than one have been observed in wash floods (Fr of 2.1) [*Rahn*, 1967], and in relatively smooth rivers with high sediment yields (Fr of 1.7) [*Montgomery et al.*, 1999]. Although beds with *Fr* greater than two (some runs with λ/D of 1 and 5) could represent local hydraulic conditions in channels, they did not approximate the reach-averaged Froude numbers that have been observed in natural streams (see section 6 for discussion).

[28] The ratio of the mobile to immobile grain sizes (D/D_{50m}) in our experiments falls within the range of values for D/D_{50m} in steep steams. For example, in the Rio Cordon, the D_{90} of the bed grain size distribution was relatively immobile during a flood with a recurrence interval of 50–60 years [*Lenzi*, 2004]. The bed D_{90} could represent the grain size of the relatively immobile sediment in the Rio Cordon. Over a range of flows in this stream, the ratio of the bed D_{90} to the transported D_{50} was between 4 and 9.4 [*Lenzi*, 2004] while in our experiments D/D_{50m} was 8.

[29] Fine gravel (3.7 mm in diameter) was fed constantly from a rotating auger apparatus through a screen to spread the gravel evenly across the flume (Figure 5). Water discharge per unit width (q) was constant (0.0049 m^2/s) for all runs while the sediment feed rate varied from 9 to 192 g m^{-1} s^{-1}. We periodically measured the sediment discharge at the flume outlet with a stopwatch and scale. We waited until the flume bed was in equilibrium with the sediment supply (sediment flux out of the flume equaled the sediment feed rate) to measure the flow depth and the height of the gravel deposit.

[30] We surveyed three to four cross sections in each run with a point gauge mounted on a sliding frame above the flume. The cross sections were in a test section (in the center of the flume length) in which the flow was fully developed and was independent of the entrance (flow gate and sediment feed) and exit conditions (no flow gate). In this section, the water and depositional surfaces were also (within the error of our measurements), on average, parallel to the flume slope. We surveyed cross sections in two different locations relative to the spheres: directly across rows of spheres and in the intervening sections between spheres. For each cross section, U was the discharge divided by the cross-sectional area.

[31] At the end of each run we measured the surface of the gravel deposit and the sphere tops in downstream transects with a point gauge. Sphere protrusion was calculated as the difference between the reach-averaged sphere

Table 2. Experimental Conditions[a]

Run	λ/D	q_s, g m^{-1} s^{-1}	A_m/A_T, %	P, %	h_a, cm	$h_a/(D-z_m)$	U, m/s	Fr	Re
1	1.02	9	24 ± 1	31 ± 1	0.7 ± 0.0	0.8	0.66 ± 0.05	2.4	4417
2	1.02	37	28 ± 2	28 ± 1	0.8 ± 0.0	0.9	0.64 ± 0.01	2.3	4379
3	1.02	71	32 ± 2	26 ± 1	0.8 ± 0.0	1.0	0.62 ± 0.01	2.2	4380
4	1.02	121	41 ± 2	21 ± 1	0.5 ± 0.0	0.9	0.92 ± 0.08	4.0	4510
5	1.02	170	50 ± 3	16 ± 1	0.6 ± 0.0	1.2	0.80 ± 0.03	3.3	4402
6	1.02	192	58 ± 3	13 ± 1	0.8 ± 0.0	2.0	0.63 ± 0.02	2.3	4382
7	1.67	18	72 ± 1	31 ± 2	1.2 ± 0.2	1.3	0.45 ± 0.08	1.3	4779
8	1.67	35	67 ± 1	40 ± 3					
9	1.67	63	71 ± 1	33 ± 2	1.4 ± 0.1	1.4	0.36 ± 0.02	1.0	4433
10	1.67	111	76 ± 3	20 ± 4	1.0 ± 0.0	1.8	0.47 ± 0.01	1.5	4378
11	1.67	173	83 ± 1	15 ± 2	1.0 ± 0.1	2.2	0.51 ± 0.06	1.6	4531
12	2.03	10	64 ± 3	86 ± 2	1.4 ± 0.1	0.5	0.40 ± 0.02	1.1	4975
13	2.03	21	73 ± 0	68 ± 1	1.1 ± 0.1	0.5	0.44 ± 0.03	1.3	4422
14	2.03	34	78 ± 0	49 ± 1	1.1 ± 0.0	0.7	0.46 ± 0.00	1.4	4378
15	2.03	47	78 ± 0	44 ± 1	1.2 ± 0.1	0.9	0.43 ± 0.03	1.3	4446
16	2.03	87	81 ± 0	32 ± 1	1.1 ± 0.1	1.2	0.44 ± 0.02	1.3	4437
17	5.08	12	37 ± 2	99 ± 1	1.0 ± 0.1	0.3	0.57 ± 0.04	1.8	5072
18	5.08	36	42 ± 2	99 ± 1	1.0 ± 0.1	0.3	0.56 ± 0.04	1.8	5081
19	5.08	54	41 ± 2	99 ± 1	0.8 ± 0.1	0.3	0.72 ± 0.03	2.5	5194
20	5.08	88	41 ± 2	99 ± 1	0.9 ± 0.0	0.3	0.62 ± 0.01	2.1	5055
21	5.08	121	55 ± 3	96 ± 3	0.9 ± 0.1	0.3	0.61 ± 0.02	2.0	4979
22	5.08	173	61 ± 3	95 ± 2	0.8 ± 0.1	0.3	0.68 ± 0.05	2.4	5111

[a]The discharge (0.0049 m^2/s), bed slope (0.10), sphere diameter (0.03 m), flume width (0.15 m), and gravel size (0.0037 m) remained the same in all runs. Here λ is the spacing between spheres, D is the sphere diameter, z_m is the height of mobile sediment, q_s is the sediment feed rate, P is the percentage of the total sphere diameter that is above the gravel deposit (protrusion), A_m is the area of the bed occupied by mobile sediment, A_T is the total bed area, h_a is the average flow depth, Re is the Reynolds number (using U and h_a), and Fr is the Froude number (using U and h_a). We did not measure the hydraulics in experiment 8. Reported uncertainties are standard errors.

top and the reach-averaged gravel surface, divided by the sphere diameter (Table 2). The bed area that was covered by gravel was calculated using equations (5), (7), and (8) and the average gravel height for each run. The proportion of the bed covered by gravel was equation (8) divided by the total bed area (5). We used the Method of Moments [e.g., *Rastetter et al.*, 1992] to correct for the errors associated with using average values in nonlinear equations (protrusion and coverage). We also calculated the standard errors for protrusion and coverage using first-order, second-moment error propagation. The gravel deposit completely covered the bottom layer of spheres (Figure 6) for most of the runs (except Runs 12, 13 and 18–22). When the bottom spheres (closely packed bed) were largely exposed (Runs 18–22), we included them in stress-partitioning and area calculations (see Appendix A). In runs 12 and 13, only small areas of the bottom spheres were exposed. We measured these areas and included them in the calculations of gravel coverage for runs 12 and 13.

[32] We determined the drag coefficient for the gravel (C_m) from a separate set of experiments (with only gravel) in which we measured the discharge and flow depth. We then set equations (2) and (3) equal and solved these equations for C_m (found to be 0.047 ± 0.004) using our measured values of S, h_a, and U. In these experiments, the relative submergence of the gravel (0.7–2.6) was similar to that in our runs with gravel and spheres (1.5–3.7). An increase in the relative submergence may be expected to decrease C_m but we did not observe such a trend within the error of our measurements.

4.2. Experimental Results

[33] The gravel gradually deposited downstream and filled the areas between the spheres and also partially buried the spheres. Although the sediment supply rate was constant, the sediment flux out of the flume varied considerably. At sufficiently high sediment supply rates, the sphere protrusion declined to 10–20% and gravel bars formed. These bars emerged from the flow, caused the channel to narrow significantly, and altered the roughness from predominantly spheres to predominantly bed forms. The bars formed adjacent to the flume walls, which could indicate that wall resistance was important at high sediment feed rates. Thus only experiments without bar forms are discussed in this paper. We also did not visually observe any secondary flows in the runs that we present below. We now examine how sediment supply and λ/D affect the sphere protrusion, bed coverage by gravel, and flow hydraulics.

4.2.1. Effects of Sediment Supply on Sediment Deposition and Flow Hydraulics

[34] We assumed that an increase in sediment supply would cause sediment deposition, a smoother bed and therefore higher flow velocities. In theory, nonlinear sediment transport processes would have amplified these small velocity increases to produce large variations in sediment flux. Thus we expected that large differences in the sediment feed rate would cause relatively small changes in the flow velocity and depth.

[35] For a given λ/D, increases in sediment supply resulted in decreased sphere protrusion (Figure 7a) and increased bed coverage by gravel (Figure 7b), as expected. An increase in sediment supply generally increased gravel coverage when λ/D was low and reduced sphere protrusion (except for λ/D of 5) when λ/D was high. For a given λ/D, sphere protrusion and coverage by gravel generally varied monotonically with sediment supply. The monotonic relationships changed with λ/D because of the variable pocket size (between spheres) for gravel deposition. There were two deviations from these regular relationships. The lowest

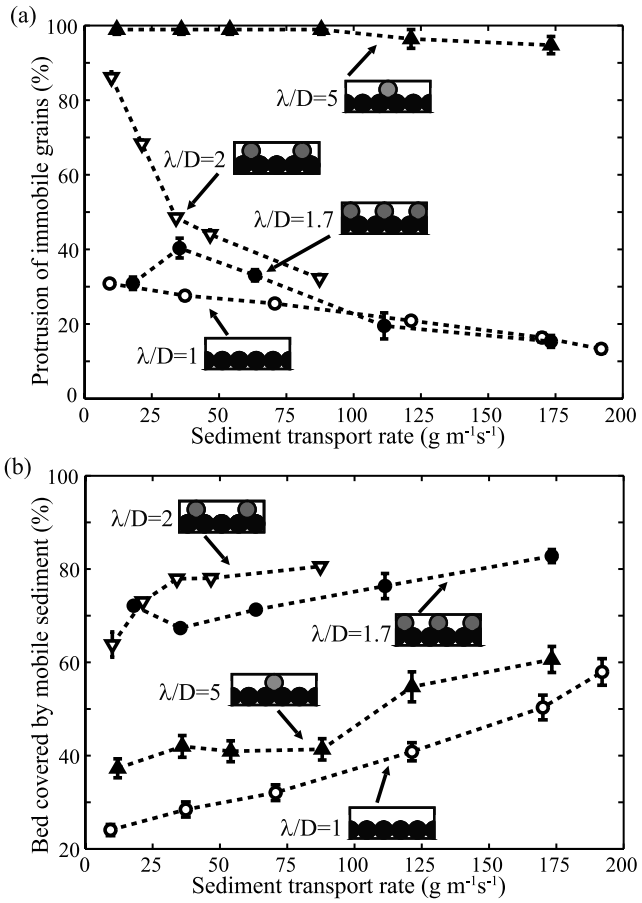

Figure 7. (a) Measured sphere protrusion and (b) coverage by mobile sediment as functions of the sediment supply and sphere spacing. Each symbol represents a different sphere spacing, which is illustrated in cross section by the corresponding diagrams.

sediment supply run for λ/D of 1.7 had an anomalously large amount of sediment deposition (high bed coverage by gravel and low sphere protrusion). Chance fluctuations in the sediment feed rate could have temporarily increased the amount of sediment deposition on the bed during this run. This augmented sediment deposit may have been present during our measurements of the bed. For λ/D of 5, protrusion (of the top spheres) only varied slightly because most of the gravel was deposited on the bottom layer of spheres.

[36] Although gravel coverage increased and sphere protrusion declined with sediment supply, we did not observe the expected change in the flow hydraulics. Neither the mean velocity nor the average flow depth showed a consistent trend with gravel supply (Figure 8). The expected small changes in velocity and average flow depth were probably indiscernible because of measurement errors. The standard errors for U and h_a (Table 2) were primarily a result of the variability of U and h_a among cross sections. Additional error could have been caused by measuring an unsteady water surface with a point gauge. The competing effects of form drag (from spheres) and skin friction (of spheres and gravel) in our experiments may have forced the velocity to remain constant with sediment supply (for a given λ/D). A higher sediment supply reduced the form resistance (through lower sphere protrusion) but augmented the reach-averaged skin friction (through higher gravel coverage) because gravel is rougher than smooth spheres.

4.2.2. Effects of Sphere Spacing on Sediment Deposition and Flow Hydraulics

[37] For a given sediment supply, decreasing λ/D from 5 to 2 (addition of spheres), caused the bed coverage by gravel to increase (Figure 7b) and the sphere protrusion to decline (Figure 7a). When λ/D decreased further from 2 to 1, the gravel coverage declined. Beds with an intermediate sphere spacing (λ/D of 2 and 1.7) had the highest gravel

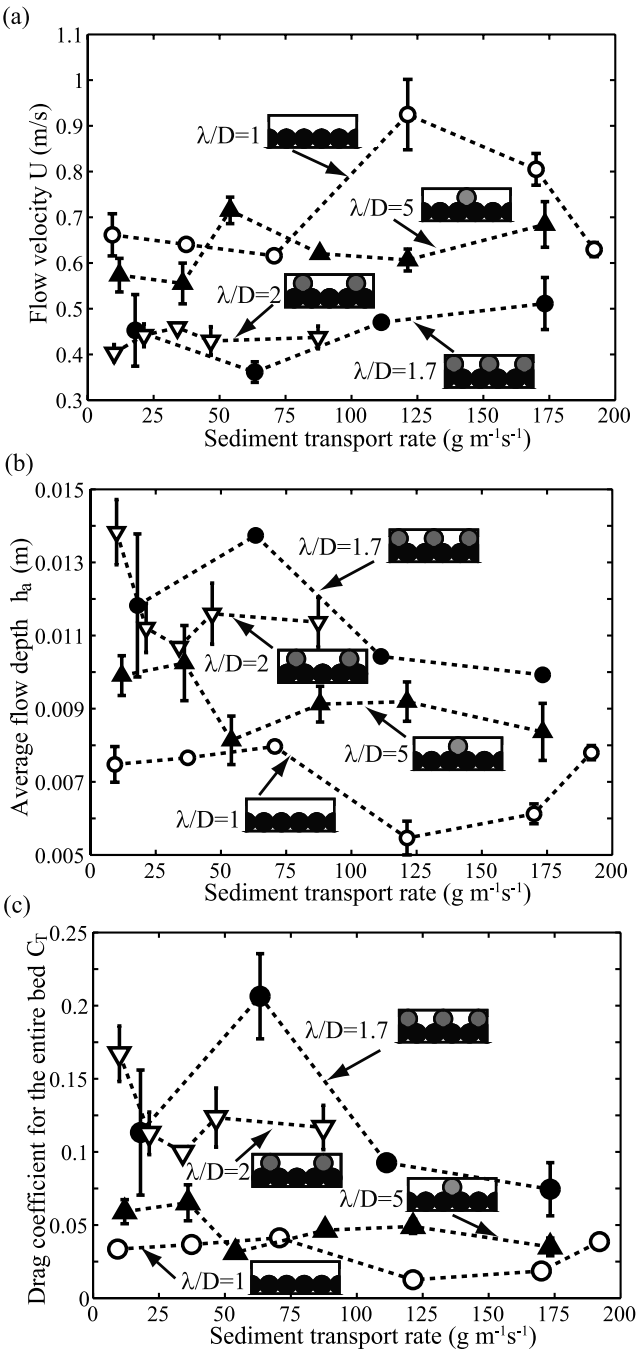

Figure 8. (a) Measured flow velocity, (b) average flow depth, and (c) drag coefficient for the entire bed as functions of the sediment supply and sphere spacing.

Table 3. Measured and Predicted Flow Velocity, Flow Depth, and Sediment Transport Rate for Each Run[a]

Run	λ/D	q_s, g m^{-1} s^{-1}	*Ackers and White* [1973] q_s	Ackers-m[a] q_s	FLvB m[a] (equation (22)) q_s	Measured U, m/s	This paper (equation (13)) U, m/s	Measured h_a, cm	This paper (equation (13)) h_a, cm
1	1.02	9	20	5	24	0.66 ± 0.05	0.45	0.7 ± 0.0	1.09
2	1.02	37	27	8	36	0.64 ± 0.01	0.47	0.8 ± 0.0	1.05
3	1.02	71	33	11	46	0.62 ± 0.01	0.48	0.8 ± 0.0	1.03
4	1.02	121	49	20	80	0.92 ± 0.08	0.51	0.5 ± 0.0	0.97
5	1.02	170	69	36	131	0.80 ± 0.03	0.54	0.6 ± 0.0	0.92
6	1.02	192	84	50	177	0.63 ± 0.02	0.56	0.8 ± 0.0	0.89
7	1.67	18	57	42	158	0.45 ± 0.08	0.52	1.2 ± 0.2	0.95
8	1.67	35	39	27	110		0.50		1.01
9	1.67	63	53	38	146	0.36 ± 0.02	0.52	1.4 ± 0.1	0.96
10	1.67	111	86	69	243	0.47 ± 0.01	0.56	1.0 ± 0.0	0.89
11	1.67	173	97	81	281	0.51 ± 0.06	0.57	1.0 ± 0.1	0.87
12	2.03	10	37	23	96	0.40 ± 0.02	0.49	1.4 ± 0.1	1.01
13	2.03	21	36	28	117	0.44 ± 0.03	0.49	1.1 ± 0.1	1.02
14	2.03	34	46	36	141	0.46 ± 0.00	0.51	1.1 ± 0.0	0.98
15	2.03	47	50	39	152	0.43 ± 0.03	0.51	1.2 ± 0.1	0.97
16	2.03	87	67	54	200	0.44 ± 0.02	0.54	1.1 ± 0.1	0.92
17	5.08	12	35	13	52	0.57 ± 0.04	0.49	1.0 ± 0.1	1.02
18	5.08	36	43	17	69	0.56 ± 0.04	0.50	1.0 ± 0.1	0.99
19	5.08	54	41	16	65	0.72 ± 0.03	0.50	0.8 ± 0.1	1.00
20	5.08	88	42	17	67	0.62 ± 0.01	0.50	0.9 ± 0.0	1.00
21	5.08	121	64	34	125	0.61 ± 0.02	0.53	0.9 ± 0.1	0.93
22	5.08	173	77	46	164	0.68 ± 0.05	0.55	0.8 ± 0.1	0.90

[a]Predicted flow velocity is given in m/s, flow depth is given in cm, and sediment transport rate is given in g m^{-1} s^{-1}; m[a] indicates that the mobile coverage and, when applicable, the stress on the mobile sediment were used to calculate sediment transport rates. FLvB is the Fernandez Luque – Van Beek equation.

coverage because they were the roughest. We calculated the drag coefficient for the entire bed (C_T) for each run from the measured values of U and h_a. We set equation (2) equal to (3), replaced C_m with C_T, and solved for C_T. Beds with an intermediate spacing (λ/D of 2 and 1.7) had higher values of C_T (Figure 8c) than beds with a very high or low spacing (λ/D of 1 and 5), as expected from previous studies of roughness (see section 3.1). The flow hydraulics (U and h_a) in our experiments seemed to be controlled more by λ/D than by sediment supply.

[38] Beds with λ/D of 1.7 and 2 not only had the highest form roughness, but also probably had the greatest skin friction because of high gravel coverage. Furthermore, the form roughness of the closely packed bed of spheres was probably less than the skin friction of the gravel. When this bed was exposed (λ/D of 1 and 5), C_T (Figure 8c) was often less than or equal to C_m (0.047). The geometric arrangement of spheres could also explain some of the differences in protrusion and coverage between beds. For example, a bed with λ/D of 2 contained more relatively flat areas for gravel deposition (thus higher gravel coverage and sphere protrusion) than did a bed with λ/D of 1 (thus lower gravel coverage and sphere protrusion).

5. Prediction of Flow and Sediment Transport Rates

[39] We used the measured sphere diameter and spacing, gravel size, channel slope, water discharge and height of the gravel deposit in combination with our stress-partitioning equations to predict the flow conditions (U and h_a). We also tested five resistance equations that were developed for steep, rough channels [*Bathurst*, 1978; *Jarrett*, 1984; *Rice et al.*, 1998; *Thompson and Campbell*, 1979; *Bathurst*, 2002]. In each resistance equation, we used (12) and the measured discharge to iteratively solve for the flow depth and therefore the hydraulic radius and flow velocity (see Appendix C and Table 3).

[40] We then used the measured grain size and the stress on the mobile sediment (equation (3)), predicted from stress partitioning, in equation (22) to predict the sediment flux for each run. We converted these dimensionless sediment transport rates into sediment mass fluxes per unit width with (19), and multiplied by the density of sediment (ρ_s). The flow velocity, average flow depth, and total shear stress predicted from stress partitioning (equation (13)) were also used in a number of other sediment transport equations (Appendix C). These sediment transport equations [*Ackers and White*, 1973; *Fernandez Luque and Van Beek*, 1976; *Bagnold*, 1980; *Parker et al.*, 1982; *Smart*, 1984] were chosen to span a range of equation forms and derivations.

[41] As a first step, we assumed constant values for C_I (0.4), C_m (0.047), τ_c^* (0.045), and τ_{cm}^* (0.045). We used the stress-partitioning equations in Appendix A when the bottom layer of spheres (C_B equal to 0.4) was exposed. The only calibrated parameter in our stress-partitioning equations was C_m, which we measured in another set of experiments with only gravel (see section 4.1).

5.1. Hydraulic Predictions

[42] The measured values of U (Figure 9) and h_a (Figure 10) generally had a large amount of scatter compared to the range of values predicted from stress partitioning (equation (13)). Part of this discrepancy could have been due to measurement errors. The difference between the predicted and observed hydraulics could have also been due to our assumption of a constant drag coefficient for the immobile grains (see section 6).

[43] The equations of *Jarrett* [1984] and *Thompson and Campbell* [1979] consistently had the highest RMSE (for

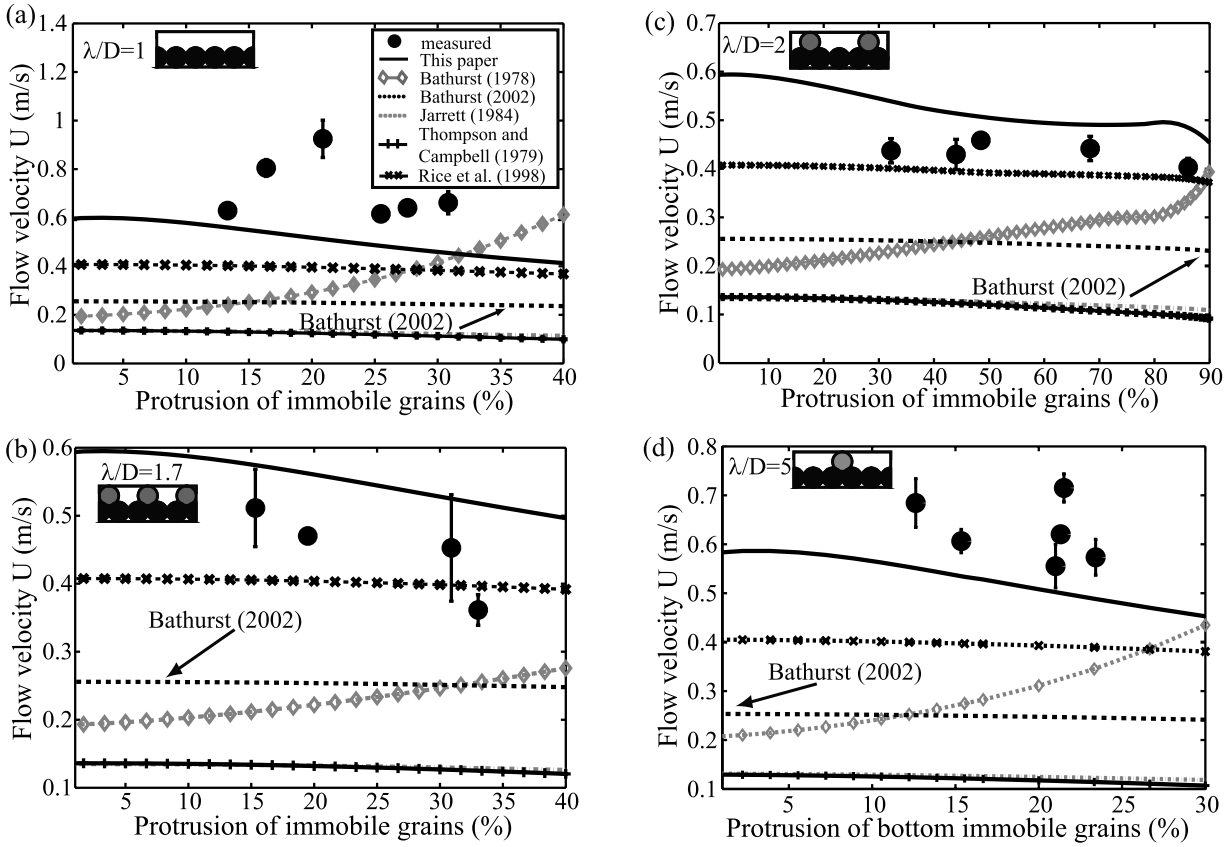

Figure 9. Predicted (lines) and measured (symbols) flow velocities as functions of the sphere protrusion for λ/D of (a) 1, (b) 1.7, (c) 2, and (d) 5. Each line represents a different resistance equation (see legend).

both U and h_a, see Table 4) of all of the resistance equations that we tested. Our stress-partitioning equation had the lowest prediction errors for U and h_a (RMSE of 0.15 m/s and 0.0015 m, respectively) while Rice's equation [*Rice et al.*, 1998] had slightly higher errors (0.22 m/s and 0.0037 m). When λ/D was 1.7 or 2, Rice's equation had similar errors to our stress-partitioning approach but it predicted nearly constant velocities between all of the runs. Because of its empirical derivation, it was difficult to determine why Rice's equation performed better than the other resistance equations. Most of these equations indirectly account for the effects of large grains by using the relative submergence. Although Rice's equation [*Rice et al.*, 1998] may be suitable to make hydraulic predictions, it does not give the stress on the mobile fraction to aid sediment flux calculations.

5.2. Sediment Transport Predictions

[44] The modified Fernandez Luque–Van Beek equation (22) predicted sediment fluxes to within an order of magnitude (factor of ten) of the measured values (Table 3) for all 22 data points. Furthermore, equation (22) predicted the observed relationship between sediment supply and sphere protrusion for each λ/D (Figure 11). For a given sphere protrusion, equation (22) also captured the relative magnitude of the measured sediment fluxes for different beds of spheres (λ/D). Errors in the predicted sediment fluxes were relatively large (Table 4) for λ/D of 1.7 and 2 (intermediate number of spheres) and relatively small for λ/D of 1 and 5 (see section 6).

[45] Most of the sediment transport equations that we tested, except for Ackers-White and (22), predicted nearly constant sediment flux with increasing sphere protrusion (Figure 11). When the sphere protrusion was relatively low, most of the sediment transport equations that we tested predicted sediment fluxes to within an order of magnitude of the measured values. The majority of these equations overpredicted the sediment flux by at least an order of magnitude when sphere protrusion was high and gravel availability was low.

[46] Unlike the other sediment transport equations that we tested, which use the total shear stress (calculated from the flow depth), Ackers-White and equation (22) assume that sediment flux is a nonlinear function of velocity ($U^{2.5}$ and U^3, respectively). Our stress-partitioning equations predicted a large velocity decline and a small depth increase with greater sphere protrusion (Figures 3a and 3b). Thus, when the sphere protrusion was high, Ackers-White and equation (22) predicted relatively low gravel fluxes because of this velocity decline, while the other sediment transport equations predicted relatively large fluxes. In steep streams, sediment transport equations that use the flow velocity may predict the sediment flux better than sediment transport equations that use the total shear stress. Velocity is mechanistically applicable for predicting sediment transport because the near-bed downstream velocity may mobilize sediment [e.g., *Nelson et al.*, 1995].

[47] *Ackers and White* [1973] had the lowest RMSE for all runs although the modified Fernandez Luque–Van Beek

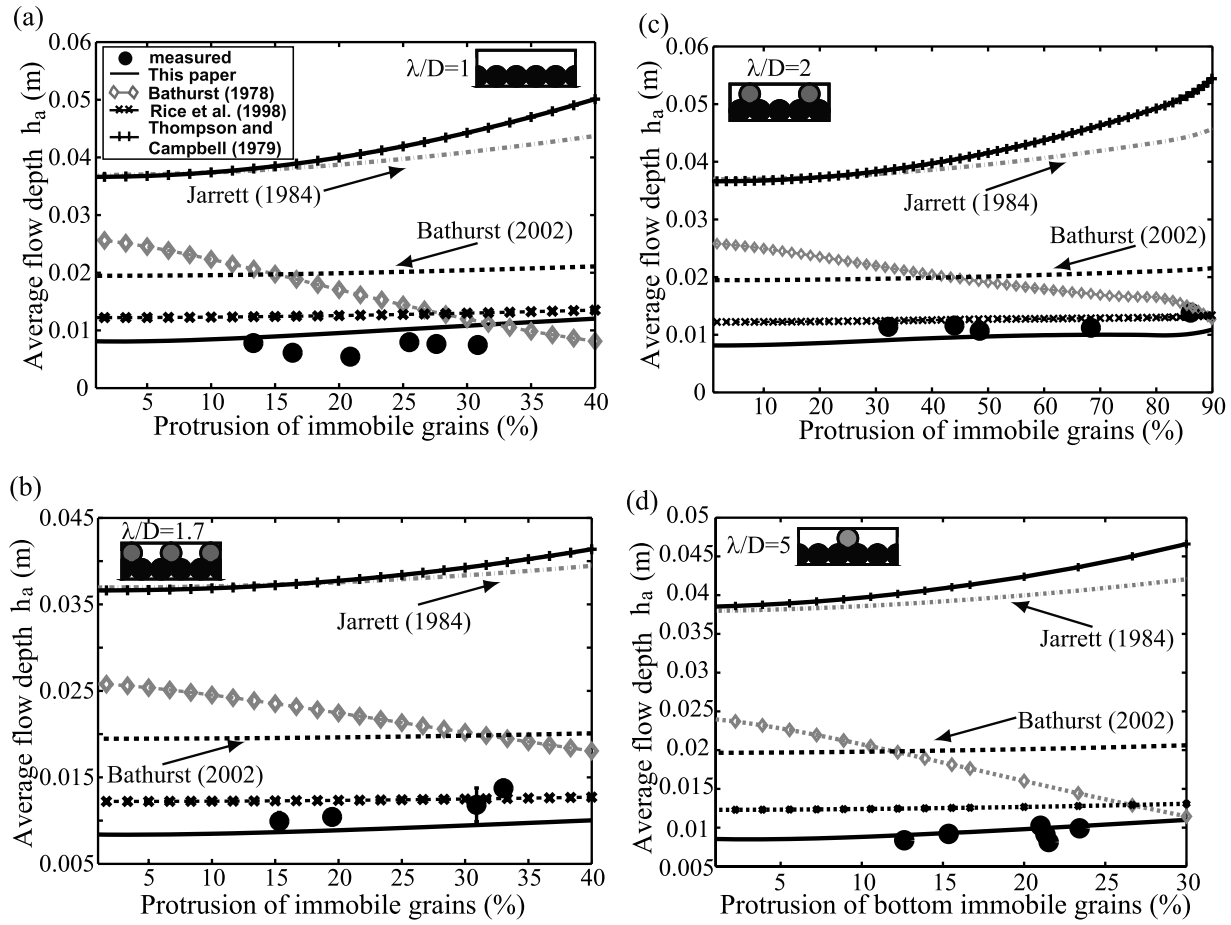

Figure 10. Predicted (lines) and measured (symbols) hydraulic radius as functions of the sphere protrusion for λ/D of (a) 1, (b) 1.7, (c) 2, and (d) 5. Each line represents a different resistance equation (see legend).

Table 4. Root-Mean-Square Error of the Predicted Velocity, Average Flow Depth, and Sediment Transport Rate

	λ/D = 1	λ/D = 1.7	λ/D = 2	λ/D = 5	All beds
	Sediment Transport, g m^{-1} s^{-1}				
Ackers and White [1973]	69	40	17	51	49
Ackers and White-mobile	94	48	17	72	66
Bagnold [1980]	194	225	250	215	220
Bagnold-mobile	31	152	180	57	117
Fernandez Luque and Van Beek [1976]	479	420	502	460	467
Fernandez Luque and Van Beek-mobile (equation (22))	27	110	102	24	74
Parker et al. [1982]	2095	2273	2467	2390	2305
Parker-mobile	101	387	86	65	199
Smart [1984]	787	784	840	798	801
Smart-mobile	79	304	230	99	194
	Velocity, m s^{-1}				
Bathurst [1978]	0.41	0.23	0.17	0.33	0.31
Bathurst [2002]	0.48	0.20	0.19	0.38	0.35
Jarrett [1984]	0.60	0.32	0.31	0.50	0.47
Rice et al. [1998]	0.34	0.07	0.05	0.24	0.22
Stress partitioning (this paper, equation (13))	0.24	0.10	0.08	0.13	0.15
Thompson and Campbell [1979]	0.60	0.32	0.32	0.51	0.47
	Average Flow Depth, cm				
Bathurst [1978]	0.95	1.04	0.76	0.76	0.87
Bathurst [2002]	1.3	0.84	0.86	1.10	1.07
Jarrett [1984]	3.23	2.65	2.87	3.07	3.00
Rice et al. [1998]	0.57	0.17	0.14	0.36	0.37
Stress partitioning (this paper, equation (13))	0.17	0.22	0.11	0.05	0.15
Thompson and Campbell [1979]	2.42	2.71	3.19	3.31	3.21

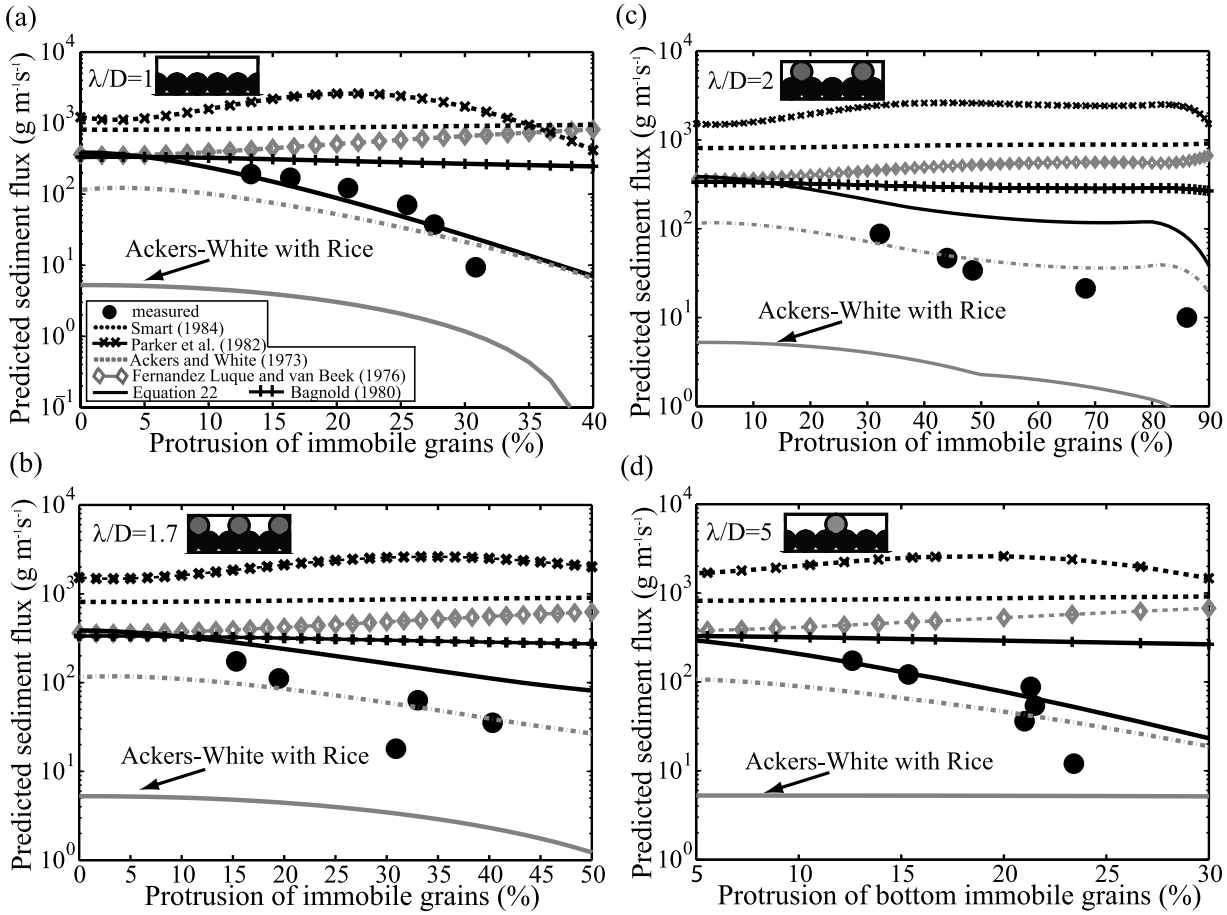

Figure 11. Predicted (lines) and measured (symbols) sediment transport rates as functions of the sphere protrusion for λ/D of (a) 1, (b) 1.7, (c) 2, and (d) 5. Each line represents a different sediment transport equation (see legend). Predicted sediment transport rates are from the original forms of the transport equations.

equation (22) had the lowest error for beds with λ/D of 1 and 5 (Table 4). Ackers-White was originally derived to use the flow velocity instead of the shear stress and cannot be modified to use the stress on the mobile sediment. However, this equation approximately incorporates the stress on the mobile sediment by using the velocity predicted from our stress-partitioning equations. Ackers-White predicted the sediment flux fairly accurately only when it used our predicted velocity. For example, the resistance equation of *Rice et al.* [1998] predicted the measured flow velocity in our experiments relatively well. When Ackers-White used the predicted flow velocity from *Rice et al.* [1998], it systematically underpredicted the measured sediment fluxes by at least an order of magnitude (Figure 11).

[48] We modified each of the sediment transport equations that we tested [*Ackers and White*, 1973; *Bagnold*, 1980; *Parker et al.*, 1982; *Smart*, 1984] to include the stress on the gravel rather than the total shear stress (when applicable, see Appendix C) and the measured gravel coverage. When modified for sphere roughness and local gravel availability, all of these equations performed better (lower RMSE) except for Ackers-White (Table 4). In addition, all of these sediment transport equations, except for Bagnold, predicted that an increase in sphere protrusion would cause a sharp decline in the sediment flux (Figure 12). The sediment flux predicted by the Bagnold equation varied relatively little with protrusion because this equation could not be modified to include the stress borne by gravel.

6. Discussion

[49] A modified sediment transport equation (22) predicts sediment fluxes to within an order of magnitude (factor of 10) of the measured values, and captures the observed relationship between sediment supply and sphere protrusion. Except for Ackers-White, all of the other sediment transport equations that we tested do not capture this relationship and significantly overpredict sediment flux. Most sediment transport equations will perform better in steep channels if they account for the effects of the large, relatively immobile grains and the limited availability of the more mobile sediment. We recommend using either the modified Ackers-White or Fernandez Luque–Van Beek (22) equations to predict sediment transport in steep streams because they had relatively low RMSE. In our experiments, Ackers-White predicted the sediment flux better than the modified Fernandez Luque–Van Beek equation. However, the modified Fernandez Luque–Van Beek equation may be more mechanistically applicable because it uses the stress borne by the mobile sediment. Our stress-partitioning equations have little empirical calibration and, with some modification, may apply to a wide range of bed conditions. One

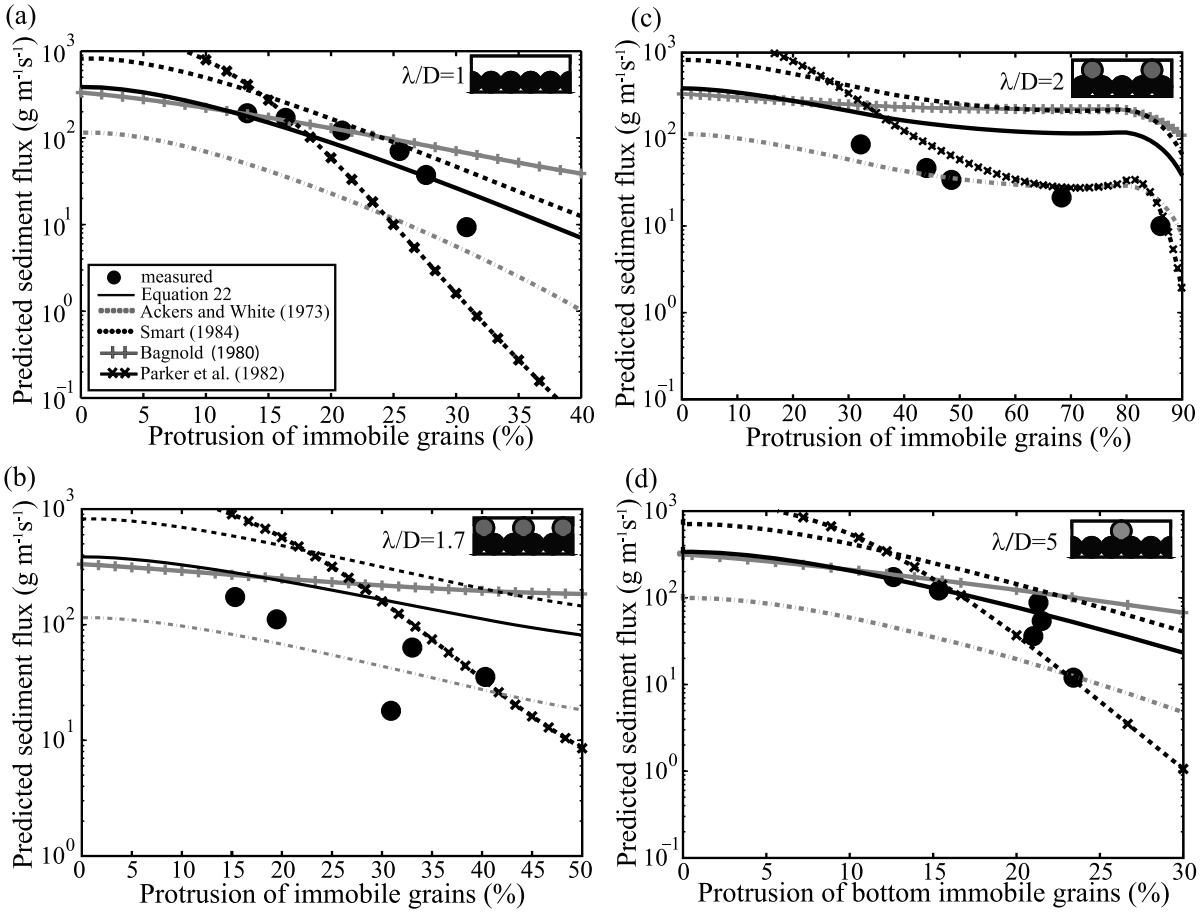

Figure 12. Predictions from modified sediment transport equations (lines) and measured (symbols) sediment transport rates as functions of the sphere protrusion for λ/D of (a) 1, (b) 1.7, (c) 2, and (d) 5. Each line represents a different sediment transport equation (see legend). Sediment transport equations are modified to include the coverage by mobile sediment and, when applicable, the stress on the mobile fraction.

caveat to our recommendation is that we only tested a small number of sediment transport equations using one set of simplified flume experiments, and not data from natural channels.

[50] The Froude numbers in some of our experiments (when λ/D was 1 or 5) were significantly higher than those expected for reach-averaged values in natural streams. In steep streams, such relatively smooth flow probably only occurs over locally exposed bedrock or directly upstream of steps. Our Froude numbers may have been lower if we included rough immobile grains, plunging and pooling flow around steps, channel bends, and woody debris. The inclusion of such forms of resistance in our experiments would have precluded a definitive test of our relatively simple sediment transport equation. Although the general relationships between sediment supply, protrusion and gravel coverage are similar in all of our runs, we do not recommend applying these exact patterns (Figure 7) to steep streams. However, the influence of sediment supply and immobile grain spacing on reach-averaged sediment deposition should be relatively independent of the Froude number.

[51] We demonstrate that, holding all other parameters constant, immobile grain protrusion and bed coverage by mobile sediment vary with sediment supply. Thus, for a given channel reach, immobile grain protrusion and coverage by gravel may serve as proxies for the local sediment availability. For calculations of sediment transport in steep streams, the next priority may be to develop a theory that predicts the immobile grain protrusion, bed coverage and grain size of mobile sediment for a given sediment supply. Such a theory could predict the effects of sediment supply on the bed roughness, grain texture and possibly aquatic habitat. Steep streams must be included in calculations of sediment routing through drainage basins because they are temporary sources or sinks of sediment. A theory that accounts for the interactions between the sediment supply and channel bed could aid such basin-scale calculations.

[52] The immobile grain spacing may be one of the most important parameters to measure when characterizing the bed of steep streams. Furthermore, the immobile grain spacing may also be important in lower-gradient channels. In such channels, gravel is sometimes added to sediment-starved reaches (below dams) to augment the deposition of sediment patches used for spawning. We found that an intermediate spacing between immobile grains caused the greatest amount of sediment deposition. Therefore addition of immobile grains to sediment-starved reaches may cause gravel retention that would otherwise not occur.

[53] We made a number of assumptions that may contribute to the performance of the Ackers-White equation and equation (22). Although we used the reach-averaged stress on the mobile sediment to predict sediment transport rates, the local deviations in stress (e.g., bursts and sweeps) and the

near-bed downstream velocity actually mobilize sediment [*Nelson et al.*, 1995]. In our experiments, the flow velocity and depth varied significantly between cross sections. These spatial variations in the flow impact the local deposition and erosion of sediment and probably influence the reach-averaged sediment transport rates. Such spatial variations in shear stress and grain size cannot be predicted accurately for steep streams. Although our assumption of uniform flow is only applicable over the scale of a reach, it appears to work well in simplified flume experiments.

[54] Although we assumed that C_I is constant, the additional effects of immobile grain protrusion, submergence and spacing, hydraulic jumps, and free-surface effects may change the flow field around the immobile grains and could cause this coefficient to vary [e.g., *Keulegan*, 1938; *Flammer et al.*, 1970; *Chanson*, 1996; *Nepf*, 1999; *Wallerstein et al.*, 2002]. For example, the value of C_I was probably lower than 0.4 for the closely packed bed of spheres because of the overlap of sphere wakes. Thus, when λ/D was 1 or 5, the assumed values of C_B and C_I may have contributed to our large prediction errors in U and h_a. Furthermore, in some of the runs with λ/D of 1.7 or 2, the Froude number was very close to critical and hydraulic jumps were evident downstream of each sphere. Such free-surface effects can significantly increase the drag coefficient of the spheres [e.g., *Flammer et al.*, 1970] above our assumed value of 0.4. In these runs, a higher drag coefficient would reduce the predicted sediment transport rates to more closely approximate the measured values. Furthermore, the drag coefficient for a sphere in the turbulent boundary layer near the bed may be larger (0.76) than our assumed value of 0.4 [*Schmeeckle*, 1998]. Additional experiments to estimate the variation of C_I with λ/D may improve our predictions of sediment transport rates for this set of experiments. They will not, however, enhance the applicability of our sediment transport equation to natural rivers where many other factors may influence C_I. Thus, until we can predict the variation of C_I, we may need to calibrate it to field measurements (Appendix B).

[55] We assumed a commonly used value for the critical shear stress because measurement of incipient motion was beyond the scope of our experiments. The predicted sediment fluxes are very sensitive to the choice of the critical shear stress when grains are near entrainment. The dimensionless critical shear stress of the relatively mobile sediment probably has a similar value in steep channels to that in lower-gradient streams [*Buffington and Montgomery*, 1997]. The apparent critical shear stress may be artificially large [e.g., *Bathurst et al.*, 1987] in steep channels because large, immobile grains reduce the portion of the total shear stress that is borne by the mobile sediment. Thus the apparent critical shear stress of the mobile sediment needs to be corrected for the effects of the immobile grains.

[56] In theory, a modified hiding function [e.g., *Einstein*, 1950; *Egiazaroff*, 1965; *Parker et al.*, 1982; *Wilcock and Southard*, 1988; *Ashworth and Ferguson*, 1989; *Parker*, 1990; *Ashworth et al.*, 1992; *Kunle*, 1980; *Wilcock*, 1993; *Wathen et al.*, 1995; *Wilcock and Crowe*, 2003] for steep streams may achieve similar results to our combined stress-partitioning and sediment transport equations. The hiding function would need to empirically account for the preferential mobility of the finer sediment and immobility of the larger grains at all but the highest flows. It would also need to use a large apparent critical shear stress [*Buffington and Montgomery*, 1997] for the finer sediment to predict the observed low sediment transport rates in steep streams. We suggest that this approach, although potentially useful, may not be as mechanistic as our stress-partitioning theory.

[57] We must make a number of modifications to our theory of stress partitioning and sediment transport before we can apply it in the field. Our sediment transport equation only has two grain types (mobile and immobile) while in rivers, the same grain may be mobile or immobile depending on the stage. Our field experience suggests that these two grain types are often visually distinct and the largest sizes on the bed (such as the commonly used D_{84} of the grain size distribution) would be immobile at most stages.

[58] Immobile grains are often not isolated roughness elements; they are arranged into clusters and steps. To include steps in our theory, we could use closely packed immobile grains in the cross-stream direction that have a characteristic downstream spacing equal to the step spacing. We would need to alter the equations for the area and volume of immobile grains to calculate the flow over a stepped or clustered bed. Although the immobile grain (or step) spacing and protrusion may vary locally [e.g., *Zimmermann and Church*, 2001], their reach-averaged values should be adequate to predict mean sediment transport rates. The definitions of step height and spacing vary considerably in the literature and a general definition is needed to unify these measurements between streams and researchers [*Nickolotsky and Pavlowsky*, 2007]. For example, protrusion could be the average distance from the immobile grain tops to the mobile sediment immediately upstream of steps. The average downstream immobile grain (or step) spacing could be the total reach length divided by the number of immobile grains within the reach.

[59] We also may need to include the effects of hydraulic jumps, spill resistance and pooling flow, which cause considerable energy losses in step-pool channels [e.g., *Hayward*, 1980; *Zimmermann and Church*, 2001; *Curran and Wohl*, 2003]. Such local variations in the flow may also alter the local and reach-averaged sediment transport rates. We neglect steps of woody debris, which can bear a significant portion of the total shear stress. Our stress-partitioning equations will need to incorporate the resistance due to large woody debris when these roughness elements are present in significant quantities. Our modified bed load equation, like many sediment transport equations, does not directly account for the flow resistance caused by moving sediment [e.g., *Bagnold*, 1956; *Owen*, 1964; *Fernandez Luque and Van Beek*, 1976; *Whiting and Dietrich*, 1990; *McEwan et al.*, 1999; *Schmeeckle and Nelson*, 2003]. With modifications, equation (22) should be able to predict the sediment flux through any steep reach when supplied with the streambed characteristics and the flow discharge.

7. Conclusions

[60] We have developed a sediment transport equation for steep boulder bed channels that includes the effects of sediment availability and immobile grain roughness. This equation implies that the bed coverage by mobile sediment and the protrusion of large, relatively immobile grains should serve as proxies for the local availability of sediment for transport. To test these assumptions, we conducted a set

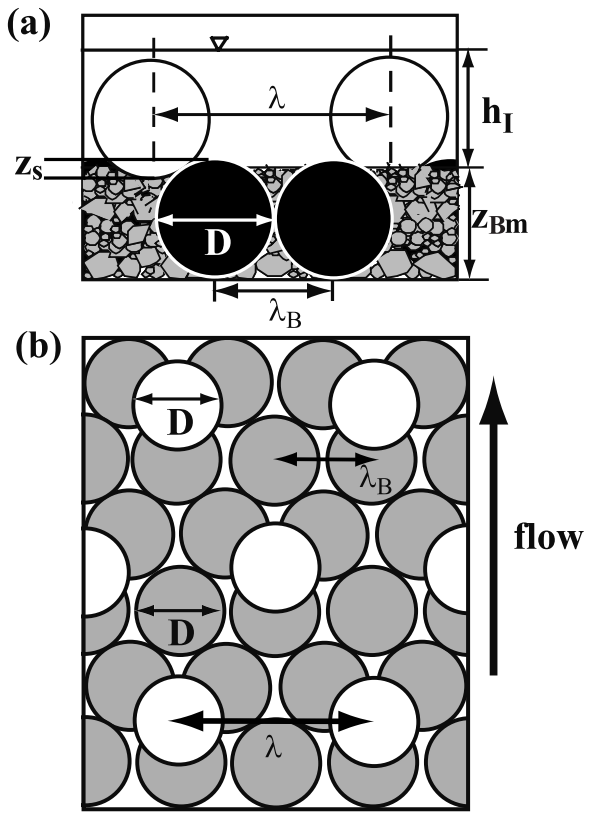

Figure A1. Idealized (a) cross-section and (b) plan view of a steep boulder bed channel that includes a bottom layer of immobile grains. Here z_s is the height of the bottom layer of immobile grains, z_{Bm} is the height of sediment from the base of the bottom grains, h_I is the flow depth above the base of the top immobile grains, and λ_B is the spacing between the bottom grains. See Figure 2 for an explanation of all other variables.

of flume experiments that simulated sediment transport in steep channels. Our flume experiments demonstrated that bed coverage by mobile sediment and immobile grain protrusion vary with sediment supply. Unlike the other sediment transport equations that we tested, our modified sediment transport equation predicted sediment fluxes to within an order of magnitude of the measured values in our flume experiments. Before generally applying our sediment transport equation to steep channels, we need to test it in more complex, natural streams.

Appendix A: Equations With Bottom Layer of Closely Packed Spheres

[61] The bottom layer of closely packed spheres is included in the stress-partitioning calculations when it is exposed to the flow (see Figure A1). When the bottom layer is fully covered by gravel, all of the equations below reduce to those in section 2. Equations (2)–(5), (11), (12), and (14)–(22) remain unaltered from section 2. When equation (1) includes the bottom layer of spheres it becomes

$$\tau_t = \frac{\tau_I A_{IP} + \tau_m A_m + \tau_B A_{BP}}{A_t}, \tag{A1}$$

where τ_B is the stress borne by the bottom layer of spheres and A_{BP} is the total bed-parallel area of the bottom spheres. Here τ_B is the drag force of the bottom spheres divided by their total bed-parallel area:

$$\tau_B = \frac{\rho A_{BF} C_B U^2}{2A_{BP}}, \tag{A2}$$

where C_B is the drag coefficient for, and A_{BF} is the bed-perpendicular area of, the bottom spheres. The bed-perpendicular area of the top spheres (A_{IF}), formerly equation (6), is now given by

$$A_{IF} = \left[\left(h_I + z_I - \frac{D}{2}\right)\sqrt{(h_I + z_I)D - (h_I + z_I)^2} + \frac{D^2}{4}\sin^{-1}\left(2\left(\frac{h_I + z_I}{D}\right) - 1\right)\right]\frac{w}{\lambda} - \left[\left(z_I - \frac{D}{2}\right)\sqrt{z_I D - z_I^2} + \frac{D^2}{4}\sin^{-1}\left(\frac{2z_I}{D} - 1\right)\right]\frac{w}{\lambda} \quad \text{when } h_I + z_I \le D \tag{A3a}$$

$$A_{IF} = \left[\frac{\pi D^2}{8} - \left(z_I - \frac{D}{2}\right)\sqrt{z_I D - z_I^2} - \frac{D^2}{4}\sin^{-1}\left(\frac{2z_I}{D} - 1\right)\right]\frac{w}{\lambda} \quad \text{when } h_I + z_I \ge D, \tag{A3b}$$

where z_I is the bed-perpendicular height of the average bed surface that is above the base of the top layer of spheres (to replace z_m) and h_I is the portion of the flow depth that is above the base of the top layer of spheres. We assume that the top and bottom spheres have the same diameter. The bed-parallel area of the top spheres (A_{IP}), equation (7), is now

$$A_{IP} = \frac{\pi D^2 w}{4\lambda} \quad \text{when } z_I/D \le 0.5 \tag{A4a}$$

$$A_{IP} = \pi D\left(z_I - \frac{z_I^2}{D}\right)\left(\frac{w}{\lambda}\right) \quad \text{when } z_I/D \ge 0.5. \tag{A4b}$$

The bed-perpendicular area of the bottom spheres (A_{BF}) is given by

$$A_{BF} = \left[\left(h + z_{Bm} - \frac{D}{2}\right)\sqrt{(h + z_{Bm})D - (h + z_{Bm})^2} + \frac{D^2}{4}\sin^{-1}\left(2\left(\frac{h + z_{Bm}}{D}\right) - 1\right)\right]\left(\frac{w\lambda}{\lambda_B^2}\right) - \left[\left(z_{Bm} - \frac{D}{2}\right)\sqrt{z_{Bm}D - z_{Bm}^2} + \frac{D^2}{4}\sin^{-1}\left(\frac{2z_{Bm}}{D} - 1\right)\right]\cdot\left(\frac{w\lambda}{\lambda_B^2}\right) \quad \text{when } h + z_{Bm} \le D \tag{A5a}$$

$$A_{BF} = \left[\frac{\pi D^2}{8} - \left(z_{Bm} - \frac{D}{2}\right)\sqrt{z_{Bm}D - z_{Bm}^2} - \frac{D^2}{4}\sin^{-1}\left(\frac{2z_{Bm}}{D} - 1\right)\right]\left(\frac{w\lambda}{\lambda_B^2}\right) \quad \text{when } h + z_{Bm} \ge D, \tag{A5b}$$

where z_{Bm} is the height of mobile sediment from the base of the bottom layer of spheres. The total number of bottom spheres within the bed area (5) is the product of λ/λ_B and w/λ_B where λ is the top-sphere spacing and λ_B is the bottom-sphere spacing. The bed-parallel area of the bottom spheres (A_{BP}) is

$$A_{BP} = \frac{\pi D^2}{4}\left(\frac{w\lambda}{\lambda_B^2}\right) \qquad \text{when } z_{Bm}/D \le 0.5 \tag{A6a}$$

$$A_{BP} = \pi D\left(z_{Bm} - \frac{z_{Bm}^2}{D}\right)\left(\frac{w\lambda}{\lambda_B^2}\right) \qquad \text{when } z_{Bm}/D \ge 0.5, \tag{A6b}$$

where z_{Bm} is

$$z_{Bm} = \text{ must be provided by user when } z_m \text{ is zero} \tag{A7a}$$

$$z_{Bm} = D - z_s + z_m \qquad \text{when } 0 < z_m < z_s \tag{A7b}$$

$$z_{Bm} = D \qquad \text{when } z_m \ge z_s, \tag{A7c}$$

and where z_s is the maximum distance that the bottom layer of spheres protrudes into the top sphere layer. Equation (A7) transforms the reference level for the mobile sediment deposit from the base of the top layer to the base of the bottom layer of spheres. It is derived from vertically packing two layers of spheres. z_{Bm} must be input by the researcher when z_m is equal to zero, and is equal to D when the mobile sediment completely covers the bottom spheres. The maximum height of the bottom immobile layer (z_s) is given by

$$z_s = D - \frac{\sqrt{3}D}{2} \tag{A8}$$

and is from the geometry of two vertically packed layers of spheres. In our experiments the top layer of spheres was not completely flush with the bottom layer and we measured z_s directly for λ/D of 2 ($D - 0.785D$) and 5 ($D - 0.841D$). The average bed surface below the top layer of spheres (z_I) is given by

$$z_I = \frac{\pi\sqrt{z_s D - z_s^2}}{\sqrt{3}\lambda_B^2}\left(\frac{\pi D^2}{8} - \left(\frac{D}{2} - z_s\right)\sqrt{z_s D - z_s^2} - \frac{D^2}{4}\sin^{-1}\left(1 - \frac{2z_s}{D}\right)\right) \qquad \text{when } z_{Bm} < D - z_s \tag{A9a}$$

$$z_I = z_m\left(1 - \frac{2A_{BP}}{\sqrt{3}w\lambda}\right) + \left(\frac{2A_{BP}}{\sqrt{3}w\lambda}\right)\left(\frac{\frac{\pi D^2}{8} - \left(z_{Bm} - \frac{D}{2}\right)\sqrt{z_{Bm}D - z_{Bm}^2} - \frac{D^2}{4}\sin^{-1}\left(\frac{2z_{Bm}}{D} - 1\right)}{2\sqrt{z_{Bm}D - z_{Bm}^2}} + z_m\right) \qquad \text{when } D > z_{Bm} > D - z_s \tag{A9b}$$

$$z_I = z_m \qquad \text{when } z_{Bm} \ge D. \tag{A9c}$$

When the mobile sediment deposit does not inundate the top spheres, z_I (A9a) is only the average height of the bottom spheres. When the mobile sediment deposit partially covers both layers of spheres, z_I (A9b) is the area-weighted average of the height of the mobile sediment and of the bottom spheres. When the mobile sediment completely covers the bottom spheres, z_I reduces to z_m (A9c).

[62] The flow depth is measured from the top of the mobile sediment deposit. We must calculate h_I when the mobile sediment deposit does not reach the base of the top spheres:

$$h_I = h - \frac{\sqrt{3}D}{2} + z_{Bm} \qquad \text{when } z_{Bm} < \frac{\sqrt{3}D}{2} \tag{A10a}$$

$$h_I = h \qquad \text{when } z_{Bm} \ge \frac{\sqrt{3}D}{2}. \tag{A10b}$$

We assume two vertically flush layers of spheres and subtract the portion of the flow depth that is below the top immobile layer (A10a). Again, when λ/D is 2 or 5, the spheres were not completely flush in our experiments, and in place of $\sqrt{3}/2$ we use 0.785 and 0.841, respectively. The bed area occupied by the mobile fraction (A_m), given by (8), is now

$$A_m = \left(\frac{\sqrt{3}\lambda w}{2} - A_{IP} - A_{BP} + A_o\right), \tag{A11}$$

where we add the bed area occupied by both layers of spheres (A_o) because it is subtracted twice from the total area. A_o is given by

$$A_o = 2A_{BP}\left(1 - \frac{\sqrt{3}}{\pi}\right)\frac{\lambda_B^2}{\lambda^2} \tag{A12}$$

and depends on the exposed bed-parallel area of the bottom spheres. The total water volume, given by (9), becomes

$$V_w = \left(\frac{\sqrt{3}h\lambda w}{2} - V_I - V_B\right), \tag{A13}$$

where V_B is the volume occupied by the bottom spheres and is given by:

$$V_B = \pi h\left(z_{Bm}(D - z_{Bm} - h) + h\left(\frac{D}{2} - \frac{h}{3}\right)\right)\left(\frac{w\lambda}{\lambda_B^2}\right) \qquad \text{when } h + z_{Bm} < D \tag{A14a}$$

$$V_B = \frac{\pi}{6}\left(D^3 - 3z_{Bm}^2 D + 2z_{Bm}^3\right)\left(\frac{w\lambda}{\lambda_B^2}\right) \qquad \text{when } h + z_{Bm} > D. \tag{A14b}$$

The volume of the top spheres, given by (10), becomes

$$V_I = \pi h_I\left(z_m(D - z_m - h_I) + h_I\left(\frac{D}{2} - \frac{h_I}{3}\right)\right)\left(\frac{w}{\lambda}\right) \qquad \text{when } h_I + z_m < D \tag{A15a}$$

$$V_I = \frac{\pi}{6}\left(D^3 - 3z_m^2 D + 2z_m^3\right)\left(\frac{w}{\lambda}\right). \qquad \text{when } h_I + z_m > D \tag{A15b}$$

When we combine equations (2)–(5), (11), (12), (A1) and (A2) and solve for the discharge per unit width, (13) becomes

$$q = \sqrt{\frac{8gSV_w^3}{3w^2\lambda^2(A_{IF}C_I + A_{BF}C_B + A_mC_m)}}. \quad (A16)$$

Appendix B: Predictions' Dependence on q, S, C_I, and C_m

[63] Our predictions of flow and sediment transport also depend on the discharge, slope and two drag coefficients. The flow velocity, stress on the mobile grains, sediment transport rate, and flow depth increase with greater discharge. At most discharges, equation (14) predicts sediment fluxes that are an order of magnitude larger (Figure B1b) than those predicted by equation (22). The flow velocity, stress on the mobile grains, and sediment transport rate increase as the gradient becomes steeper. At lower gradients, immobile grain protrusion has a large effect on the sediment flux but as slope increases the influence of protrusion declines (Figure B1c). When the slope is less than 10%, the sediment fluxes predicted by (14) and (22) can differ by at least an order of magnitude (Figure B1d).

[64] The apparent value of C_I may vary with the immobile grain submergence, spacing and protrusion. For example, C_I could vary between 0.4 (for a sphere) and 1.2 (for a cylinder) as immobile grains emerge from the flow. An increase in C_I decreases the flow velocity, the stress on the mobile sediment, and the sediment flux. The influence of C_I on the predicted sediment flux increases with greater immobile grain protrusion and lower immobile grain spacing (Figure B1e). When C_I increases from 0.4 to 1.2, the difference between the sediment fluxes predicted from equations (14) and (22) can increase by three orders of magnitude (Figure B1f).

[65] Although the value of C_m in natural, steep channels is relatively unknown, we expect it to vary with the relative submergence and grain size of the mobile sediment as suggested by Keulegan-type relationships for grain resistance [e.g., *Keulegan*, 1938]. The velocity, stress on the mobile sediment and sediment transport rate increase with greater C_m (Figure B1g). Many of the predicted changes in sediment flux with q, S, C_I and C_m are caused by the total stress and the stress on the mobile sediment approaching the critical stress. Thus the critical shear stress, which is relatively unknown for steep streams, will strongly influence sediment flux predictions.

Appendix C: Resistance and Sediment Transport Equations

[66] *Bathurst* [1978] empirically calibrated the resistance equation of *Judd and Peterson* [1969] to account for the effects of large roughness elements. He gives

$$\frac{U}{\sqrt{gRS}} = \left(\frac{8}{f}\right)^{\frac{1}{2}} = \left(\frac{R}{0.365D_{84}}\right)^{2.34}\left(\frac{w}{d}\right)^{7(\lambda_1-0.08)} \quad \text{where } \lambda_1 = \frac{\sum A_F}{A_{bed}}, \quad (C1)$$

where f is the friction factor, d is the average flow depth, A_F is the frontal cross-sectional area of large grains and A_{bed} is the total bed area. We substitute equation (5) for A_{bed} and (6) for A_F and use the flow depth between the spheres (h) for d. Equation (C1) is applicable when $R/D_{84} < 1$. *Thompson and Campbell* [1979] developed a resistance equation for a channel paved with large boulders:

$$\frac{8gRS}{U^2} = f = \left(\left(1 - \frac{0.1k_s}{R}\right)2\log\left(\frac{12R}{k_s}\right)\right)^{-2}, \quad (C2)$$

where k_s is Nikuradse's roughness coefficient (here $4.5D_{50}$), and D_{50} is the median grain size of the boulders. *Jarrett* [1984] empirically fit an equation (to predict Manning's n) to data from channels with gradients less than 3.4%. His equation, when modified to solve for the friction factor, is

$$\frac{U}{\sqrt{8gRS}} = \left(\frac{1}{f}\right)^{\frac{1}{2}} = 0.4R^{0.33}S^{-0.38}. \quad (C3)$$

Rice et al. [1998] developed this roughness equation for riprap paved channels:

$$\frac{U}{\sqrt{gRS}} = \left(\frac{8}{f}\right)^{\frac{1}{2}} = 5.1\log\left(\frac{d}{D_{84}}\right) + 6, \quad (C4)$$

where we replace D_{84} with D. *Bathurst* [2002] empirically fit a power law to data measured in streams with bed slopes between 0.8% and 4%:

$$\frac{U}{\sqrt{gRS}} = \left(\frac{8}{f}\right)^{\frac{1}{2}} = 3.10\left(\frac{d}{D_{84}}\right)^{0.93}, \quad (C5)$$

where d is the average flow depth and we replace D_{84} with D. In all of the above equations we substitute equation (12) for U. In equations (C4) and (C5) we use h_a for d. The discharge, channel slope, height of the mobile sediment, and immobile grain spacing and diameter are used to iteratively solve each resistance equation for h_a and U.

[67] *Ackers and White* [1973] used flume experiments to calibrate a total load (suspended and bed load) equation that is based on the shear velocity. We use the coarse sediment version where the mobility number (F_{gr}) is

$$F_{gr} = \frac{U}{\sqrt{gD_{50}\left(\frac{\rho_s}{\rho} - 1\right)}}\frac{1}{\sqrt{32}\log\left(\frac{10h_a}{D_{50}}\right)}, \quad (C6)$$

and we substitute D_{50m} for the grain size (D_{50}). The dimensionless sediment transport rate (q_s^*) is given by

$$q_s^* = 0.025\frac{U}{\sqrt{gD_{50}\left(\frac{\rho_s}{\rho} - 1\right)}}\left(\frac{F_{gr}}{0.17} - 1\right)^{1.5}, \quad (C7)$$

which we convert to a volumetric sediment transport rate (q_s) per unit width with

$$q_s = q_s^*\left[\left(\frac{\rho_s}{\rho} - 1\right)gD_{50}^3\right]^{0.5} \quad (C8)$$

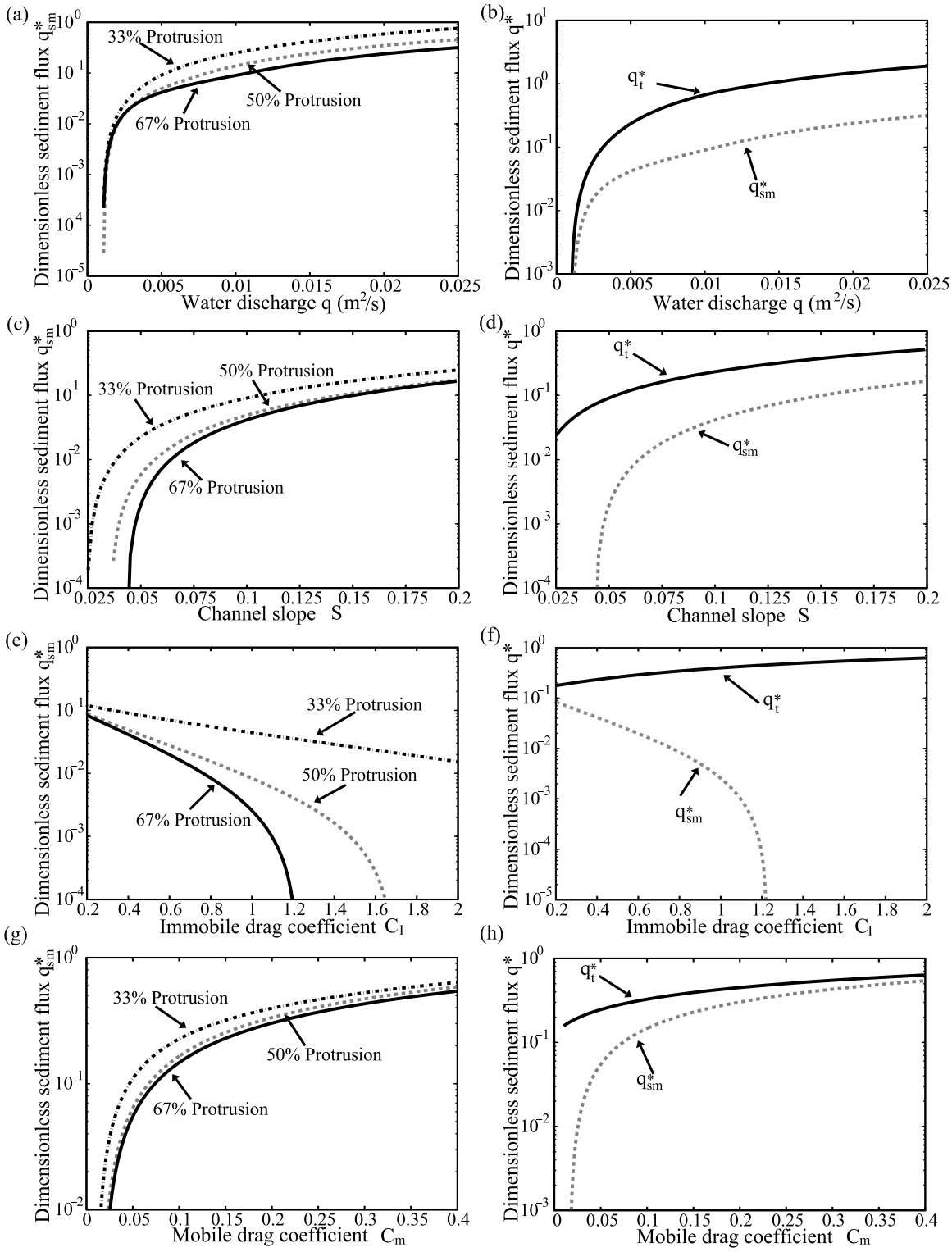

Figure B1. Sample predictions of dimensionless sediment transport rates. The transport rates predicted by our modified equation (22) are shown (for three values of protrusion) as functions of (a) discharge per unit width, (c) channel slope, (e) drag coefficient for the immobile grains, and (g) drag coefficient for the mobile sediment. The transport rates predicted by our modified equation (22) and the original Fernandez Luque and Van Beek equation (14) are shown as functions of (b) discharge per unit width, (d) channel slope, (f) drag coefficient for the immobile grains, and (h) drag coefficient for the mobile sediment. All variables, except for those shown in each plot, are held constant. Reference values are λ/D of 2, q of 0.0049 m^2/s, S of 0.10, C_m of 0.047, C_I of 0.4, D_{50m} of 0.0037 m, and τ_c^* of 0.045.

and multiply by ρ_s to obtain a mass flux per unit width. We then modify (C8) to account for the availability of mobile sediment (proportion of bed covered by mobile sediment),

$$q_{sm} = q_s \frac{A_m}{A_T}. \tag{C9}$$

Smart [1984] empirically calibrated a transport equation to steep (3–25%) flume experiments:

$$q_s^* = 4\left[\left(\frac{D_{90}}{D_{30}}\right)^{0.2} S^{0.6} \frac{U}{\sqrt{gh_a S}} \tau_t^{*0.5}(\tau_t^* - \tau_c^*)\right], \tag{C10}$$

where we substitute the immobile grain diameter (D) for D_{90} and the median size of the mobile sediment (D_{50m}) for D_{30}. We convert (C10) to a mass flux per unit width using equation (15) multiplied by ρ_s. We then modify (C10) to use the stress on, and the proportion of the bed covered by, mobile sediment:

$$q_{sm}^* = 4\left[\left(\frac{D_{90}}{D_{30}}\right)^{0.2} S^{0.6} \frac{U}{\sqrt{gh_a S}} \tau_m^{*0.5}(\tau_m^* - \tau_{cm}^*)\right]\left(\frac{A_m}{A_t}\right). \tag{C11}$$

Bagnold [1980] empirically calibrated a sediment transport equation based on stream power:

$$i_b = \frac{\rho_s i_{b*}}{(\rho_s - \rho)}\left(\frac{\omega - \omega_0}{(\omega - \omega_0)_*}\right)^{\frac{3}{2}}\left(\frac{Y}{Y_*}\right)^{-\frac{2}{3}}\left(\frac{D_b}{D}\right)^{-\frac{1}{2}}, \tag{C12}$$

where i_b has units of kg m^{-1} s^{-1}, i_{b*} is 0.1 kg m^{-1} s^{-1}, $(\omega - \omega_0)_*$ is 0.5 kg m^{-1} s^{-1}, Y_* is .01 m, D_* is 1.1×10^{-3} m, and Y is the flow depth. We substitute D_{50m} for D_b and h_a for Y. ω_0 is given by

$$\omega_0 = 5.75\left[\left(\frac{\rho_s}{\rho} - 1\right)\rho 0.04\right]^{\frac{3}{2}}\left(\frac{g}{\rho}\right)^{\frac{1}{2}} D_b^{1.5} \log\left(\frac{12Y}{D_b}\right). \tag{C13}$$

We then modify the Bagnold equation to include the limited availability of mobile sediment:

$$i_{bm} = \frac{\rho_s i_{b*}}{(\rho_s - \rho)}\left(\frac{\omega - \omega_0}{(\omega - \omega_0)_*}\right)^{\frac{3}{2}}\left(\frac{Y}{Y_*}\right)^{-\frac{2}{3}}\left(\frac{D_b}{D_*}\right)^{-\frac{1}{2}}\left(\frac{A_m}{A_t}\right) \tag{C14}$$

Parker et al. [1982] used data from Oak Creek to calibrate a sediment transport equation that uses the subsurface grain size. Our experiments fall into the range of $0.95 < \phi_{50} < 1.65$ [*Parker et al.*, 1982] and we therefore use

$$W^* = 0.0025 \exp\left[14.2(\phi_{50} - 1) - 9.28(\phi_{50} - 1)^2\right], \tag{C15}$$

where ϕ_{50} is given by

$$\phi_{50} = \frac{\tau_{50}^*}{\tau_{r50}^*} \tag{C16}$$

and where τ_{r50}^* is 0.0876. τ_{50}^* is given by (20) for the stress on the mobile sediment and (16) for the total stress. We modify the Parker equation to include the stress on, and bed covered by, mobile sediment

$$W_m^* = 0.0025 \exp\left[14.2(\phi_{50} - 1) - 9.28(\phi_{50} - 1)^2\right]\left(\frac{A_m}{A_t}\right). \tag{C17}$$

[68] Some of the above equations use the hydraulic radius, which we did not use in our stress-partitioning equations. The hydraulic radius (R) is normally the cross-sectional area of the flow divided by the wetted perimeter. Here we calculate the hydraulic radius as the total water volume (equation (9) or (A13)) divided by the total wetted-surface area. The total wetted-surface area (A_w) is given by

$$A_W = \frac{\sqrt{3} w \lambda}{2} - \frac{\pi w z_I}{\lambda}(D - z_I) - \frac{\pi w \lambda z_{Bm}}{\lambda_B^2}(D - z_{Bm}) + h\sqrt{3}\lambda - \frac{A_{IF}\lambda}{w} - \frac{A_{BF}\lambda_B}{w} + A_{IS} + A_{BS}. \tag{C18}$$

The first three terms on the right side of (C18) give the wetted-bed area occupied by mobile grains (total bed area minus the bed area of immobile grains). The fourth through sixth terms give the wetted-wall area not occupied by immobile grains (wetted-wall area minus the wetted-wall area occupied by immobile grains). The final two terms are the wetted-surface areas of the top (A_{IS}) and bottom (A_{BS}) immobile grains. A_{IS} is given by

$$A_{IS} = \pi D h_I \left(\frac{w}{\lambda}\right) \qquad \text{when } h_I + z_I \le D \tag{C19a}$$

$$A_{IS} = \pi D(D - z_I)\left(\frac{w}{\lambda}\right) \qquad \text{when } h_I + z_I \ge D. \tag{C19b}$$

A_{IS} is derived from the geometry of a sphere that is intersected by the flow depth and sediment height. A_{BS} is given by

$$A_{BS} = \pi D h \left(\frac{w\lambda}{\lambda_B^2}\right) \qquad \text{when } h + z_{Bm} \le D \tag{C20a}$$

$$A_{BS} = \pi D(D - z_{Bm})\left(\frac{w\lambda}{\lambda_B^2}\right) \qquad \text{when } h + z_{Bm} \ge D. \tag{C20b}$$

The hydraulic radius (R) is then given by

$$R = \frac{V_w}{A_w}. \tag{C21}$$

Notation

A_{IF}	bed-perpendicular area of immobile grains.
A_{IP}	bed-parallel area of immobile grains.
A_m	bed-parallel area of mobile sediment.
A_t	total bed area.
C_m	drag coefficient for the mobile sediment.
C_I	drag coefficient for the immobile grains.
C_T	drag coefficient for the entire bed.
D	immobile grain diameter.
D_{50}	median grain size of entire bed.
D_{50m}	median grain size of mobile sediment.
g	acceleration due to gravity.
h	flow depth between immobile grains.
h_a	average flow depth.

P protrusion of immobile grains (%).
p portion of immobile grains that protrude above the mobile bed surface.
q discharge per unit width.
q_s volumetric sediment transport rate per unit width.
q_s^* dimensionless sediment transport rate.
q_{sm} volumetric transport rate of mobile sediment per unit width.
q_{sm}^* dimensionless transport rate of mobile sediment.
S reach-averaged water surface slope.
U reach-averaged flow velocity.
V_I volume of immobile grains.
V_w total water volume.
w channel width.
w/λ number of immobile grains within A_t.
z_m average bed-perpendicular height of the mobile sediment above the base of the immobile grains.
λ immobile grain spacing.
λ/D dimensionless immobile grain spacing.
ρ density of water.
ρ_s density of sediment.
τ_c critical shear stress.
τ_c^* dimensionless critical shear stress.
τ_{cm} critical shear stress of mobile sediment.
τ_{cm}^* dimensionless critical shear stress of mobile sediment.
τ_I stress borne by immobile grains.
τ_m stress borne by mobile sediment.
τ_m^* dimensionless stress borne by mobile sediment.
τ_t total boundary shear stress.
τ_t^* dimensionless total boundary shear stress.

Symbols for appendixes

A_{BF} bed-perpendicular area of bottom immobile grains.
A_{BP} bed-parallel area of bottom immobile grains.
A_{BS} wetted-surface area of bottom immobile grains.
A_{IS} wetted-surface area of top immobile grains.
A_w total reach wetted-surface area.
A_o total bed-parallel area occupied by both layers of immobile grains.
C_B drag coefficient for bottom layer of immobile grains.
h_I portion of the flow depth that is above the base of the upper layer of immobile grains.
R hydraulic radius.
V_B volume of bottom immobile grains.
z_{Bm} average height of mobile sediment from the base of the bottom layer of immobile grains.
z_I average bed-perpendicular height of the bed surface (mobile sediment and bottom layer of immobile grains) measured from the base of the upper layer of immobile grains.
z_s maximum height of the bottom layer of grains measured from the base of the top layer of immobile grains.
λ_B spacing of bottom layer of immobile grains.
τ_B stress borne by bottom layer of immobile grains.

[69] **Acknowledgments.** Funding for this work was provided by the Water Resources Center of California (W-966), the National Center for Earth-Surface Dynamics and the American Geophysical Union (Horton Research Grant). J. W. Kirchner acknowledges support from the Miller Institute for Basic Research. A. Porto, J. Potter, K. Lindquist, M. Trso, and L. Sklar assisted with flume design and/or experiments. M. Stacey and L. Hsu provided helpful comments on an earlier version of this manuscript. The comments from A. Wilcox and two anonymous reviewers helped to improve the clarity and presentation of this manuscript.

References

Ackers, P., and W. W. White (1973), Sediment transport; new approach and analysis, *J. Hydraul. Div. Am. Soc. Civ. Eng.*, *99*, 2041–2060.

Adenlof, K. A., and E. E. Wohl (1994), Controls on bedload movement in a subalpine stream of the Colorado Rocky Mountains, USA, *Arct. Alp. Res.*, *26*, 77–85.

Aguirre-Pe, J. (1975), Incipient motion in high gradient open channel flow with artificial roughness elements, paper presented at 16th Congress, Int. Assoc. Hydraul. Res., Sao Paulo, Brazil.

Aguirre-Pe, J., and R. Fuentes (1990), Resistance to flow in steep rough streams, *J. Hydraul. Eng.*, *116*, 1374–1387.

Ashida, K., and M. Bayazit (1973), Initiation of motion and roughness of flows in steep channels, paper presented at 15th Congress, Int. Assoc. Hydraul. Res., Istanbul, Turkey.

Ashworth, P. J., and R. I. Ferguson (1989), Size-selective entrainment of bed load in gravel bed streams, *Water Resour. Res.*, *25*, 627–634.

Ashworth, P. J., R. I. Ferguson, P. E. Ashmore, C. Paola, D. M. Powell, and K. L. Prestegaard (1992), Measurements in a braided river chute and lobe: 2. Sorting of bed load during entrainment, transport, and deposition, *Water Resour. Res.*, *28*, 1887–1896.

Aziz, N. M., and D. E. Scott (1989), Experiments on sediment transport in shallow flows in high gradient channels, *Hydraul. Sci. J.*, *34*, 465–478.

Bagnold, R. A. (1956), The flow of cohesionless grains in fluids, *Trans. R. Soc. London, Ser. A*, *249*, 235–297.

Bagnold, R. A. (1980), An empirical correlation of bedload transport rates in flumes and natural rivers, *Proc. R. Soc. London, Ser. A*, *372*, 453–473.

Bathurst, J. C. (1978), Flow resistance of large-scale roughness, *J. Hydraul. Div. Am. Soc. Civ. Eng.*, *104*, 1587–1603.

Bathurst, J. C. (1985), Flow resistance estimation in mountain rivers, *J. Hydraul. Eng.*, *111*, 625–643.

Bathurst, J. C. (1987), Critical conditions for bed material movement in steep, boulder-bed streams, in *Erosion and Sedimentation in the Pacific Rim, The Corvallis Symposium*, edited by R. Beschta et al., *IAHS Publ.*, *165*, 309–318.

Bathurst, J. C. (2002), At-a-site variation and minimum flow resistance for mountain rivers, *J. Hydrol.*, *269*, 11–26.

Bathurst, J. C., R. M. Li, and D. B. Simons (1979), Hydraulics of mountain rivers, *Rep. CER78JCB-RML-DBS55*, Civ. Eng. Dep., Colo. State Univ., Fort Collins, Colo.

Bathurst, J. C., R. M. Li, and D. B. Simons (1981), Resistance equation for large-scale roughness, *J. Hydraul. Div. Am. Soc. Civ. Eng.*, *107*, 1593–1613.

Bathurst, J. C., W. H. Graf, and H. H. Cao (1987), Bed load discharge equations for steep mountain rivers, in *Sediment Transport in Gravel-Bed Rivers*, edited by C. R. Thorne, J. C. Bathurst, and R. D. Hey, pp. 453–477, John Wiley, Hoboken, N. J.

Buffington, J. M., and D. R. Montgomery (1997), A systematic analysis of eight decades of incipient motion studies, with special reference to gravel-bedded rivers, *Water Resour. Res.*, *33*, 1993–2029.

Byrd, T. C., and D. J. Furbish (2000), Magnitude of deviatoric terms in vertically averaged flow equations, *Earth Surf. Processes Landforms*, *25*, 319–328.

Byrd, T. C., D. J. Furbish, and J. Warburton (2000), Estimating depth-averaged velocities in rough channels, *Earth Surf. Processes Landforms*, *25*, 167–173.

Chanson, H. (1996), *Air Bubble Entrainment in Free-Surface Turbulent Shear Flows*, 348 pp., Elsevier, New York.

Curran, J. H., and E. E. Wohl (2003), Large woody debris and flow resistance in step-pool channels, Cascade Range, Washington, *Geomorphology*, *51*, 141–157.

D'Agostino, V., and M. A. Lenzi (1999), Bedload transport in the instrumented catchment of the Rio Cordon part II: Analysis of the bedload rate, *Catena*, *36*, 191–204.

Egiazaroff, I. V. (1965), Calculation of nonuniform sediment concentrations, *J. Hydraul. Div. Am. Soc. Civ. Eng.*, *91*, 225–247.

Einstein, H. A. (1950), The bedload function for sediment transport in open channel flows, *Tech. Bull. 1026*, Soil Conserv. Serv., U. S. Dep. of Agric., Washington, D. C.

Einstein, H. A., and R. B. Banks (1950), Fluid resistance of composite roughness, *Eos Trans. AGU*, *31*, 603.

Fernandez Luque, R., and R. Van Beek (1976), Erosion and transport of bedload sediment, *J. Hydraul. Res.*, *14*, 127–144.

Ferro, V. (1999), Friction factor for gravel-bed channel with high boulder concentration, *J. Hydraul. Eng.*, *125*, 771–778.

Flammer, G. H., J. P. Tullis, and E. S. Mason (1970), Free surface, velocity gradient flow past hemisphere, *J. Hydraul. Div. Am. Soc. Civ. Eng.*, *7*, 1485–1502.

Graf, W. H., and L. Suszka (1987), Sediment transport in steep channels, *J. Hydrosci. Hydraul. Eng.*, *5*, 11–26.

Hayward, J. A. (1980), Hydrology and stream sediments from Toresse stream catchment, *Spec. Publ. 17*, 236 pp., Tussock Grasslands and Mountain Lands Inst., Lincoln Univ., Christchurch, New Zealand.

Jarrett, R. D. (1984), Hydraulics of high-gradient streams, *J. Hydraul. Eng.*, *110*, 1519–1539.

Jordanova, A. A., and C. S. James (2003), Experimental study of bed load transport through emergent vegetation, *J. Hydraul. Eng.*, *129*, 474–478.

Judd, H. E., and D. F. Peterson (1969), Hydraulics of large bed element channels, *Rep. PRWG 17-6*, Utah Water Res. Lab., Utah State Univ., Logan, Utah.

Katul, G., P. Wiberg, J. Albertson, and G. Hornberger (2002), A mixing layer theory for flow resistance in shallow streams, *Water Resour. Res.*, *38*(11), 1250, doi:10.1029/2001WR000817.

Keulegan, G. H. (1938), Laws of turbulent flow in open channels, *J. Res. Natl. Bur. Stand. U.S.*, *21*, 707–741.

King, J., W. G. Nickling, and J. A. Gillies (2005), Representation of vegetation and other nonerodible elements in aeolian shear stress partitioning models for predicting transport threshold, *J. Geophys. Res.*, *110*, F04015, doi:10.1029/2004JF000281.

Kunle, R. A. (1980), Bed-surface size changes in gravel-bed channels, *J. Hydraul. Eng.*, *115*, 731–741.

Laronne, J. B., C. Garcia, and I. Reid (2001), Mobility of patch sediment in gravel bed streams: Patch character and its implication for bedload, in *Gravel-Bed Rivers V*, edited by M. P. Mosley, pp. 249–289, N. Z. Hydrol. Soc., Wellington.

Lawrence, D. S. L. (1997), Macroscale surface roughness and frictional resistance in overland flow, *Earth Surf. Processes Landforms*, *22*, 365–382.

Lawrence, D. S. L. (2000), Hydraulic resistance in overland flow during partial and marginal surface inundation: Experimental observations and modeling, *Water Resour. Res.*, *36*, 2381–2393.

Lee, A. L., and R. I. Ferguson (2002), Velocity and flow resistance in step-pool streams, *Geomorphology*, *46*, 59–71.

Lenzi, M. A. (1999), Mofologia y estabilidad de las secuencias en escalones en los torrents appinos de elevada pendiente, *Ing. Agua*, *6*, 151–162.

Lenzi, M. A. (2001), Step-pool evolution in the Rio Cordon, northeastern Italy, *Earth Surf. Processes Landforms*, *26*, 991–1008.

Lenzi, M. A. (2004), Displacement and transport of marked pebbles, cobbles and boulders during floods in a steep mountain stream, *Hydrol. Processes*, *18*, 1899–1914.

Lenzi, M. A., V. A. D'Agostino, and P. Billi (1999), Bedload transport in the instrumented catchment of the Rio Cordon part I: Analysis of bedload records, conditions and threshold of bedload entrainment, *Catena*, *36*, 171–190.

Lenzi, M. A., L. M. Mao, and F. Comiti (2006), When does bedload transport begin in steep boulder-bed streams?, *Hydrol. Processes*, *20*, 3517–3533, doi:10.1002/hyp.6168.

Lepp, L. R., C. J. Koger, and J. A. Wheeler (1993), Channel erosion in steep gradient, gravel-paved streams, *Bull. Assoc. Eng. Geol.*, *30*, 434–454.

Li, R., and H. W. Shen (1973), Effect of tall vegetations on flow and sediment, *J. Hydraul. Div. Am. Soc. Civ. Eng.*, *5*, 793–814.

Manga, M., and J. W. Kirchner (2000), Stress partitioning in streams by large woody debris, *Water Resour. Res.*, *36*, 2373–2379.

Marcus, W. A., K. Roberts, L. Harvey, and G. Tackman (1992), An evaluation of methods for estimating Manning's *n* in small mountain streams, *Mountain Res. Dev.*, *12*, 227–239.

McEwan, I. K., B. J. Jefcoate, and B. B. Willetts (1999), The grain-fluid interaction as a self-stabilizing mechanism in fluvial bed load transport, *Sedimentology*, *46*, 407–416.

Mizuyama, T. (1977), Bedload transport in steep channels, Ph.D. thesis, 118 pp., Kyoto Univ., Kyoto, Japan.

Montgomery, D. R., M. S. Panfil, and S. K. Hayes (1999), Channel-bed mobility response to extreme sediment loading at Mount Pinatubo, *Geology*, *27*, 271–274.

Morris, H. M. (1955), Flow in rough conduits, *Trans. Am. Soc. Civ. Eng.*, *120*, 373–398.

Munson, B. R., D. R. Young, and T. H. Okiishi (1998), *Fundamentals of Fluid Mechanics*, 3rd ed., 877 pp., John Wiley, New York.

Nepf, H. M. (1999), Drag, turbulence, and diffusion in flow through emergent vegetation, *Water Resour. Res.*, *35*, 479–489.

Nelson, J. M., R. L. Shreve, S. R. McLean, and T. G. Drake (1995), Role of near-bed turbulence structure in bed load transport and bed form mechanics, *Water Resour. Res.*, *31*, 2071–2086.

Nickolotsky, A., and R. T. Pavlowsky (2007), Morphology of step-pools in a wilderness headwater stream: The importance of standardizing geomorphic measurements, *Geomorphology*, *83*, 294–306.

Owen, P. R. (1964), Saltation of uniform grains in air, *J. Fluid Mech.*, *20*, 225–242.

Papanicolaou, A. N., P. Diplas, C. L. Dancey, and M. Balakrishnan (2001), Surface roughness effects in near-bed turbulence: Implications to sediment entrainment, *J. Eng. Mech.*, *127*, 211–218.

Parker, G. (1990), Surface-based bedload transport relation for gravel rivers, *J. Hydraul. Res.*, *28*, 417–436.

Parker, G., P. C. Klingemen, and D. L. McLean (1982), Bedload and size distribution in paved gravel-bed streams, *J. Hydraul. Div. Am. Soc. Civ. Eng.*, *108*, 544–571.

Rahn, P. H. (1967), Sheetfloods, streamfloods, and the formation of pediments, *Ann. Assoc. Am. Geogr.*, *57*, 593–604.

Rastetter, E. B., A. W. King, B. J. Cosby, G. M. Hornberger, R. V. O'Neill, and J. E. Hobbie (1992), Aggregating fine-scale ecological knowledge to model coarser-scale attributes of ecosystems, *Ecol. Appl.*, *2*, 55–72.

Raupach, M. R. (1992), Drag and drag partition on rough surfaces, *Boundary Layer Meteorol.*, *60*, 375–395.

Raupach, M. R., D. A. Gillette, and J. F. Leys (1993), The effect of roughness elements on wind erosion threshold, *J. Geophys. Res.*, *98*, 3023–3029.

Rice, C. E., K. C. Kadavy, and K. M. Robinson (1998), Roughness of loose rock riprap on steep slopes, *J. Hydraul. Eng.*, *124*, 179–185.

Rickenmann, D. (1994), Bedload transport and discharge in the Erlenbach Stream, in *Dynamics and Geomorphology of Mountain Rivers*, *Lecture Notes Earth Sci.*, vol. 52, edited by P. Ergenzinger and K. H. Schmidt, pp. 53–66, Springer, New York.

Rickenmann, D. (1997), Sediment transport in Swiss torrents, *Earth Surf. Processes Landforms*, *22*, 937–951.

Rosso, M., M. Schiara, and J. Berlamont (1990), Flow stability and friction factor in rough channels, *J. Hydraul. Eng.*, *116*, 1109–1118.

Rouse, H. (1965), Critical analysis of open-channel resistance, *J. Hydraul. Div. Am. Soc. Civ. Eng.*, *4*, 1–25.

Scheuerlein, H. (1973), The mechanics of flow in steep, rough open channels, paper presented at 15th Congress, Int. Assoc. Hydraul. Res., Istanbul, Turkey.

Schlichting, H. (1936), Experimentelle Untersuchungen zum Rauhigkeitsproblem, *Ingen. Arch.*, *7*, 1–34.

Schmeeckle, M. W. (1998), The mechanics of bedload sediment transport, Ph.D. dissertation, Univ. of Colo., Boulder.

Schmeeckle, M. W., and J. M. Nelson (2003), Direct numerical simulation of bedload transport using a local, dynamic boundary condition, *Sedimentology*, *50*, 279–301.

Shields, F. D., and C. J. Gippel (1995), Prediction of effects of woody debris removal on flow resistance, *J. Hydraul. Eng.*, *121*, 341–354.

Smart, G. M. (1984), Sediment transport formula for steep channels, *J. Hydraul. Eng.*, *110*, 267–276.

Stock, J., and W. E. Dietrich (2003), Valley incision by debris flows: Evidence of a topographic signature, *Water Resour. Res.*, *39*(4), 1089, doi:10.1029/2001WR001057.

Stock, J. D., and W. E. Dietrich (2006), Erosion of steepland valleys by debris flows, *GSA Bull.*, *118*, 1125–1148, doi:10.1130/B25902.1.

Stone, B. M., and H. T. Shen (2002), Hydraulic resistance of flow in channels with cylindrical roughness, *J. Hydraul. Eng.*, *128*, 500–506.

Thompson, D. M. (2007), The characteristics of turbulence in a shear zone downstream of a channel constriction in a coarse-grained forced pool, *Geomorphology*, *83*, 199–214.

Thompson, S. M., and P. L. Campbell (1979), Hydraulics of a large channel paved with boulders, *J. Hydraul. Res.*, *17*, 341–354.

Vallé, B. L., and G. B. Pasternack (2006), Air concentrations of submerged and unsubmerged hydraulic jumps in a bedrock step-pool channel, *J. Geophys. Res.*, *111*, F03016, doi:10.1029/2004JF000140.

Wallerstein, N. P., C. V. Alonso, S. J. Bennett, and C. R. Thorne (2002), Surface wave forces acting on submerged logs, *J. Hydraul. Eng.*, *3*, 349–353.

Wathen, S. J., R. I. Ferguson, T. B. Hoey, and A. Werrity (1995), Unequal mobility of gravel and sand in weakly bimodal river sediments, *Water Resour. Res.*, *31*, 2087–2096.

Whiting, P., and W. E. Dietrich (1990), Boundary shear stress and roughness over mobile alluvial beds, *J. Hydraul. Eng.*, *116*, 1495–1511.

Wiberg, P. L., and J. D. Smith (1987), Initial motion of coarse sediment in streams of high gradient, in *Erosion and Sedimentation in the Pacific*

Rim, The Corvallis Symposium, edited by R. Beschta et al., *IAHS Publ.*, *165*, 299–308.
Wiberg, P. L., and J. D. Smith (1991), Velocity distribution and bed roughness in high-gradient streams, *Water Resour. Res.*, *27*, 825–838.
Wilcock, P. R. (1993), Critical shear stress of natural sediments, *J. Hydraul. Eng.*, *119*, 491–505.
Wilcock, P. R., and J. C. Crowe (2003), Surface-based transport model for mixed-size sediment, *J. Hydraul. Eng.*, *129*, 120–128.
Wilcock, P. R., and J. B. Southard (1988), Experimental study of incipient motion in mixed-size sediment, *Water Resour. Res.*, *24*, 1137–1151.
Wilcox, A. C., and E. E. Wohl (2007), Field measurements of three-dimensional hydraulics in a step-pool channel, *Geomorphology*, *83*, 215–231.
Wilcox, A. C., J. M. Nelson, and E. E. Wohl (2006), Flow resistance dynamics in step-pool channels: 2. Partitioning between grain, spill, and woody debris resistance, *Water Resour. Res.*, *42*, W05419, doi:10.1029/2005WR004278.
Wohl, E., and D. M. Thompson (2000), Velocity characteristics along a small step-pool channel, *Earth Surf. Processes Landforms*, *25*, 353–367.
Zimmermann, A., and M. Church (2001), Channel morphology, gradient profiles and bed stresses during flood in a step-pool channel, *Geomorphology*, *40*, 311–327.

W. E. Dietrich and J. W. Kirchner, Department of Earth and Planetary Science, University of California, 307 McCone Hall, Berkeley, CA 94720, USA.

E. M. Yager, School of Geographical Sciences, Arizona State University, PO Box 870104, Tempe, AZ 85287, USA. (elowyn.yager@asu.edu)